

Bacterial filamentation: a bet for survival in stressful environments

Jesús Vélez Santiago Rafael Peña-Miller

2022-09-06T00:00:00+00:00

Table of contents

Welcome	6
Abstract	6
Acknowledgements	6
Introduction	7
1 Image processing	9
1.1 Introduction	9
1.2 Preprocessing	10
1.3 Segmentation	10
1.4 Tracking	10
1.5 Manual corrections	11
1.6 Data extraction	11
2 Experiment analysis	13
2.1 Introduction	13
2.2 General preprocessing of data	14
2.3 Results	16
2.3.1 Cell length and the amount of GFP are crucial in determining cell survival	16
2.3.2 Number of divisions and cell age do not appear to play a clear role in determining cell survival	23
2.3.3 Time to reach filamentation matters in determining cell survival	26
2.3.4 Increasing the complexity of the system and analyzing it in an unsupervised way allows a correct classification of cell states	29
2.3.4.1 Principal Component Analysis (PCA) emphasizes the importance of cell length and its GFP in cell survival	30
2.3.4.2 Uniform Manifold Approximation and Projection (UMAP) correctly represents the local structure of cell states	35
2.3.5 Population dynamics reveal how filamentation contributes cell survival	37

2.3.6	Heterogeneity in plasmid copy-number allows various forms of survival in addition to filamentation	42
2.4	Discussion	46
3	Models to the rescue; filamentation abstraction	47
3.1	Introduction	47
3.2	Filamentation model	48
3.3	Numerical results	49
3.3.1	Filamentation provides transient resistance to stressful conditions	49
3.3.2	Filamentation increases the minimum inhibitory concentration	51
3.3.3	Heterogeneity in the toxin-antitoxin system represents a double-edged sword in survival probability	52
3.4	Benefits and limitations of the model	56
4	Discussion	57
Appendix		60
Code availability	60
Software tools	60
Python	60
R	61
Julia	61
Software usage	62
Undergraduate research project	62
Cell-viewer	62
Filamentation model	62
Colophon	63
References		64

List of Figures

2.1	Cell classification and its distribution across experiments.	15
2.2	DsRed temporal distribution.	17
2.3	GFP temporal distribution.	18
2.4	Length temporal distribution.	20
2.5	Experiment's initial values.	22
2.6	Experiment's initial values differences.	23
2.7	Cell's number of divisions.	25
2.8	Time elapsed since the last division at the beginning of the experiment.	26
2.9	Time to filamentation filtered.	28
2.10	Experiment initial values with time to filamentation.	29
2.11	Principal Component Analysis of chromosomal strain.	31
2.12	Principal Component Analysis of plasmid strain.	32
2.13	Variables contribution of Principal Component Analysis of chromosomal strain.	33
2.14	Variables contribution of Principal Component Analysis of plasmid strain.	34
2.15	UMAP coordinates of chromosome strain.	36
2.16	UMAP coordinates of plasmid strain.	37
2.17	Population status over time.	39
2.18	Population measurements over time.	41
2.19	Population survivals binned by initial GFP over time.	43
2.20	Plasmid initial GFP survival probability.	44
2.21	Plasmid initial length survival probability.	45
3.1	Cell dimensions relationship.	48
3.2	Effect of filamentation on intracellular toxin concentration.	50
3.3	Effect of filamentation on minimum inhibitory concentration (MIC).	52
3.4	Variability in the toxin-antitoxin system produces different proportions of cell states.	54
3.5	Effect of variability on the toxin-antitoxin system.	55

List of Tables

1.1	Resulting data table from image processing.	11
4.1	Github repositories used for this project.	60
4.2	Packages used to built the project documents.	63

Welcome

Abstract

Scientists have extensively studied the mechanisms that orchestrate the growth and division of bacterial cells. Cells adapt their shape and dimensions in response to variations in the intracellular and extracellular environments by integrating information about the presence of nutrients or harmful agents in the decision to grow or divide. *Filamentation* is a process that occurs when rod-shaped cells stop dividing but continue to grow, thus producing elongated cells (Y. Wang et al. 2014; Y. Wang, Yin, and Chen 2014; James-Lizcano, Hunn, and Papadopoulos 2014; Sheryl S. Justice et al. 2008). Some cells can naturally grow as filamentous, while others only do so under stressful conditions (Cayron, Dedieu, and Lesterlin 2020; S. S. Justice et al. 2006). Here, we use mathematical modeling and computational simulations to evaluate a toxic agent's intracellular concentration as a function of cell length. We show that filamentation can act as a strategy that promotes the resilience of a bacterial population under stressful environmental conditions.

Acknowledgements

I offer this work with gratitude to all the people who have been part of my personal and intellectual growth. Thanks.

Introduction

Antimicrobial resistance (AMR) can be considered one of the most critical health problems of the century. That is, microorganisms' ability to grow despite exposure to substances designed to inhibit their growth or kill them. In April 2014, the World Health Organization (WHO) published its first global report on AMR surveillance ("Editorial Board" 2014). Taking out of the darkness a common fear, a possible post-antibiotic future in which common infections or minor injuries can kill. Therefore, understanding the mechanisms of avoiding antibiotic action is essential for producing knowledge and developing strategies that reduce the generation of resistant bacteria.

Bacterial adaptability to hostile environmental conditions can be explained by different elements, not necessarily exclusive. For instance, mutational phenomena that allow bacteria to evade the mechanisms of action of certain antibiotics have been one of the most studied (Dever and Dermody 1991; Andersson 2005). However, continuous technological development has allowed us to explore hypotheses where phenotypic heterogeneity is considered in detail, allowing us to study emergent behaviors in isogenic populations (Ackermann 2015). Thus, we have gone from studying bacterial communities as a whole to studying them from each of the cells that compose them and their emergent properties.

Single-cell microfluidics is one of the technologies that has made it possible to create and maintain the microenvironments necessary for studying bacteria (Yin and Marshall 2012). Among the most outstanding utilities of microfluidics, we can find the engineering of bacterial systems, microbial ecology, bacterial cell cycle, homeostasis, cell shape, and geometry. The latter is one of the characteristics that allow the study of bacterial filamentation, a phenomenon that occurs when the cell stops dividing but continues to grow, thus producing elongated cells in the form of filaments.

Mathematical modeling is among the most common strategies to address the AMR problem. Mathematical modeling allows one to pose real-life problems in a space filled with mathematical language, solve them, and test their solutions in a real-life living system (Verschaffel, Greer, and Corte 2002). Therefore, this approach can also be used to analyze in detail why a particular biological phenomenon is occurring, how its behavior can be modified, and, finally, to design specific experiments to determine their accuracy and usefulness.

This thesis describes and discusses how and why bacterial filamentation may be a general mechanism for cell survival upon exposure to toxic agents, such as antibiotics, based on experimental analyses and mathematical modeling. We divided this thesis into three chapters that explain the methodologies used and take us one step closer to understanding filamentation with each chapter.

Chapter 1 describes the fundamental process of identifying and quantifying the properties of each cell over time, for example, its length, the amount of internal toxin, and the amount of resistance to the toxin.

Chapter 2 used the data processed in the previous chapter to explore bacterial filamentation at the population and single-cell levels. Data exploration allowed us to simultaneously observe the behavior of filamentation and its properties in heterogeneous populations. For reference, one population with an antibiotic resistance gene located on the chromosome and another on multicopy plasmids.

Finally, in Chapter 3, we postulated a mathematical model that considers the relationship of cell surface area and volume to the uptake of a toxic agent diffusing into the medium. This model allowed us to specifically evaluate the effect of filamentation in an environment similar to that observed experimentally. Thus, experiments and models work together to learn more about a biological phenomenon to help understand and combat the AMR problem.

1 Image processing

1.1 Introduction

With the progress of technology, optical and fluorescence microscopy has become a fundamental tool for the characterization and understanding of the bacterial world. Microscopy has allowed humanity to extend its senses to observe the unknown world with exciting new perspectives they might never have envisioned otherwise. Furthermore, microscopy offers a clear advantage over other techniques that characterize bacteria since it can acquire data from living cells in spatial resolution ([Schermelleh et al. 2019](#)). ([Schermelleh et al. 2019](#)).

Microfluidic research techniques' mechanical and intellectual development provides an excellent opportunity to overcome bio-medical and chemical techniques ([Convery and Gadegaard 2019](#)). With the discovery of fluorescent proteins (e.g., GFP and DsRed) and improvements in fluorescent reporters, it is possible to specifically label distinctive cellular components and track cellular functions ([Specht, Braselmann, and Palmer 2017](#)). Therefore, collectively, it is possible to study communities of bacteria at the level of individual cells ([Balaban et al. 2004](#); [Elowitz et al. 2002](#)).

Although all this technological development has provided a significant advance for the scientific community in the image analysis field, extracting quantitative properties from these images is crucial. Unfortunately, it is a difficult step for analyzing experiments.

Not so long ago, image analysis in biology relied on manual quantification. However, manual analysis suffers from two main problems: 1) accuracy and 2) scalability (that is, analyzing thousands or more images). Fortunately, improvements in image accuracy and computational image analysis capabilities are revolutionizing the quantification of biological processes, reducing the manual correction required to analyze the experiments. ([Caicedo et al. 2017](#); [Smith et al. 2018](#)).

Here, we used a series of programs in μ J (<https://github.com/ccg-esb-lab/uJ>), which consists of an ImageJ macro library (mainly) for quantifying unicellular bacterial dynamics in microfluidic devices ([Schneider, Rasband, and Eliceiri 2012](#)). The specific steps we used are described below and summarized in `?@fig-something`.

1.2 Preprocessing

We exported the figures obtained by the NIS-Elements software (RRID:SCR_014329) from the microfluidics experiments in TIFF (Tagged Image File Format) format. Each figure was named as follows: *experimentxyct001*, where *experiment* indicates the name assigned to the experiment, *xy* the trap number, *c* the fluorescence channel, and *t* the passage of time.

Subsequently, we compile the images, rename them and save them as images in different folders. We maintained the classification by fluorescence channels and phase contrast, and within the channel folder, it is the sub-classification by trap number.

1.3 Segmentation

We carry out an image segmentation analysis to determine which parts of the photographs correspond to cells. *Segmentation* consists of classification at the pixel level, which allows us to define the pixels that give identity to the limit of a cell, its interior, and the image's background (everything that is not a cell). The resulting image is the *segmentation mask*, containing only the pixels that identify cells.

To build the segmentation mask, we used *Deepcell* ([Van Valen et al. 2016](#)). *Deepcell* is a network trained with a robust set of images that people previously classified as cells. However, the generation of the segmentation masks is not absolved of errors (see also Section 1.5). Sometimes we must correct them manually due to

1. mistakenly identifying two or more cells as one,
2. identifying two or more cells when there is only one cell, and
3. failing to identify a cell.

1.4 Tracking

From the image segmentation, we obtain ROI files (region of interest), which contain coordinates of the position of individual cells in each photograph ([Brinkmann 2008](#)). *Tracking* is following a region of interest in a consecutive series of images. In this case, the tracking identifies the lineages, that is, the ancestry of each cell.

We read the ROI files in Python through the *shapely* package, which efficiently reconstructs polygons, thus calculating the length of the cells ([Van Rossum and Drake 2009](#);

Gillies et al. 2007--). Also, in Python, using ROI files, we track cells with the k-nearest neighbors' algorithm that uses various cell properties, such as fluorescence intensity, length, and shape of each cell, to identify cell lineages (Altman 1992).

1.5 Manual corrections

For cell-tracking manual correction, we used *Napari*, an open-source python-based tool designed to explore, annotate, and analyze large multidimensional images (Sofroniew et al. 2021). Our custom cell-viewer allows us to easily lineage data visualization, custom-plotting, and lineage correction. Code for our cell-viewer is available on <https://github.com/ccg-esb-lab/uJ/tree/master/single-channel>.

We produced high-throughput data of thousands of cells with a single-cell resolution to the end of the lineage manual reconstruction. We obtained data on the time series of fluorescent intensity, morphological properties of individual cells (*e.g.*, elongation, duplication rate), and time-resolved population-level statistics (*e.g.*, probability of survival to the antibiotic shock).

1.6 Data extraction

We construct a file in columnar format through image processing that contains the information necessary to analyze each experiment (*i.e.*, chromosomal and plasmids) in its different traps (*i.e.*, XY identifier). See Table 1.1 for a complete description of the output data. Subsequently, the table was analyzed in R for statistical computation and plotting (see Chapter 2) (R Core Team 2022).

Table 1.1: Resulting data table from image processing.

Column	Description
experimentID	Unique identifier of the experiment.
trapID	Unique identifier of the trap used.
lineageID	Unique integer of the stem cell and its ancestry.
cellID	Unique identification number for each cell existing since the beginning of the experiment or generated later.
motherID	Unique identification number for each cell existing since the beginning of the experiment or generated later.
trackID	Indicates the x-y coordinates where the cell being tracked starts.

Column	Description
roiID	Indicates the x-y position in which the cell is located, followed after each photograph.
frame	Number of the photograph in the sequence of photographs taken, indicating the elapsed time (10 minutes per frame).
length	Cell length.
division	Indicates cell division events, represented by the value 1 when they occur and 0 otherwise.
GFP	Represents the relative fluorescence intensity in each cell by green fluorescent protein (<i>i.e.</i> , GFP).
DsRed	Represents the relative fluorescence intensity for cells generated by rhodamine's internalization (<i>i.e.</i> , DsRed); an indicator of cell death events.
tracking_score	Determine how good or bad the tracking of a cell was.
state	Indicates the state of the cell determined from its length and fluorescence thresholds. -1 for death, 0 for normal, and 1 for filamentation (see Section 2.2 for detailed information).

2 Experiment analysis

2.1 Introduction

The previous chapter (see Chapter 1) detailed the steps necessary to extract data from a set of microfluidic images through image analysis techniques and fluorescence microscopy. Each step was instrumental in creating a dataset that was easy to explore and ask questions. With the help of computational biology, systems biology, and data analysis techniques, we could process these files to help us in the search to find the role of filamentation in cell survival.

Computational biology and systems biology contributed to the development of this analysis. In principle, computational biology originated after the origin of computer science with the British mathematician and logician Alan Turing (regularly known as the father of computing) ([TURING 1950](#)). Over time, systems biology emerged as an area that synergistically combines models and experimental data to understand biological processes ([Bruggeman et al. 2007](#)). Thus, giving a step towards creating models that, in general, are phenomenological but sometimes serve to discover new ideas about the process under study. Without the computer's power, modern ideas and aspects of studying biological sciences would otherwise be unthinkable.

Here, we divide the experimental analysis into two main parts: 1) at the cell level or measurements at specific points in time and 2) at the population level and time series. The first level allowed us to identify the individual contribution of each variable under-study to determine cell survival. The second level allowed us to understand how the population behaves according to the passage of time in the face of exposure to a harmful agent (in this case, beta-lactam antibiotics). Together, both visions of the same study phenomenon allowed us to extract the main ideas for postulating a mathematical model that seeks to show how filamentation is a factor for cell survival in stressful environments (see Chapter 3).

2.2 General preprocessing of data

The raw data processing consisted mainly of creating two levels of observation for the cells of both chromosomal strains and multicopy plasmids. The first level is at a cell granularity, point properties. The second level consists of the cells over time, thus observing properties at the population level. We did this because it would allow us to understand what factors affect filamentation and why.

We normalized the fluorescence values of DsRed and GFP for both experiments based on the values observed before antibiotic exposure. It allowed us to have a basis to work with and compare expressions between cells. In the case of DsRed environment drug concentration, we also applied a logarithmic transformation to observe subtle changes in fluorescence intensity that would allow us to detect cell death.

Ultimately, we decided to classify cells into four fundamental groups based on whether the cell filamentoed and survived (see Figure 2.1). We define a *filamented cell* as a cell with more than two standard deviations from the mean concerning the lengths observed before introducing antibiotics into the system. On the other hand, although there are multiple ways to define death from single-cell observations ([Trevors 2012; Kroemer et al. 2008](#)), we considered a *cell dead or missing* when we stopped having information about it, either because of fluorescence in the red channel was above a given threshold (resulting from an increase in cell membrane permeability and the introduction of fluorescent dye into the cell) or because it left the field of observation. Therefore, we defined a *surviving cell* as a cell observed before and after antibiotic exposure that did not surpass the DsRed death threshold.

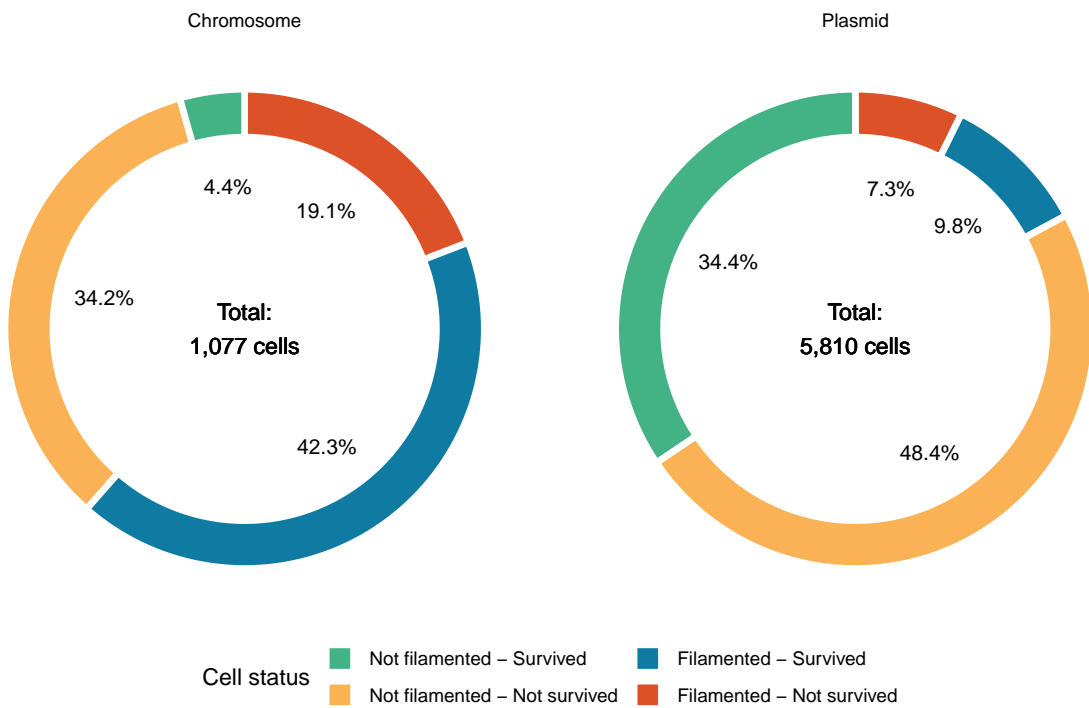


Figure 2.1: Cell classification and its distribution across experiments. We define a *filamented cell* as a cell whose length exceeded two standard deviations from the mean at any time during the experiment. A *surviving cell* is a cell we observed before and after exposure to the antibiotic and did not surpass the DsRed death threshold. Accordingly, we removed from the analysis those cells that died before or were born after antibiotic exposure. Therefore, we delimited the effect caused by antibiotic exposure.

2.3 Results

2.3.1 Cell length and the amount of GFP are crucial in determining cell survival

We evaluated the DsRed, GFP, and length values for each cell at different time points: initial, filamentation, and end. This preprocessing allowed us to observe and quantify each cell at critical times in the experiment and eliminate noise or signals outside the scope of this investigation.

We define the *initial time* as the first time we observed the cell in the experiment. *Filamentation time* equals when a cell reaches the filamentation threshold (see Figure 2.4) for the first time. We defined the *end time* as the time of the last observation of the cell. We decided to bound the end time for surviving cells to one frame (10 min) after the end of antibiotic exposure so that the observed signal would reflect the final stress responses.

When we compared the distributions of DsRed, GFP, and length for both experiments, we observed the changes in their role in cell survival. In Figure 2.2, we show that indistinctly and, as expected, surviving cells managed to eliminate the antibiotic by the end time. In contrast, dead cells presented higher levels of antibiotics (measured by proxy through the mean DsRed intensity of the cell).

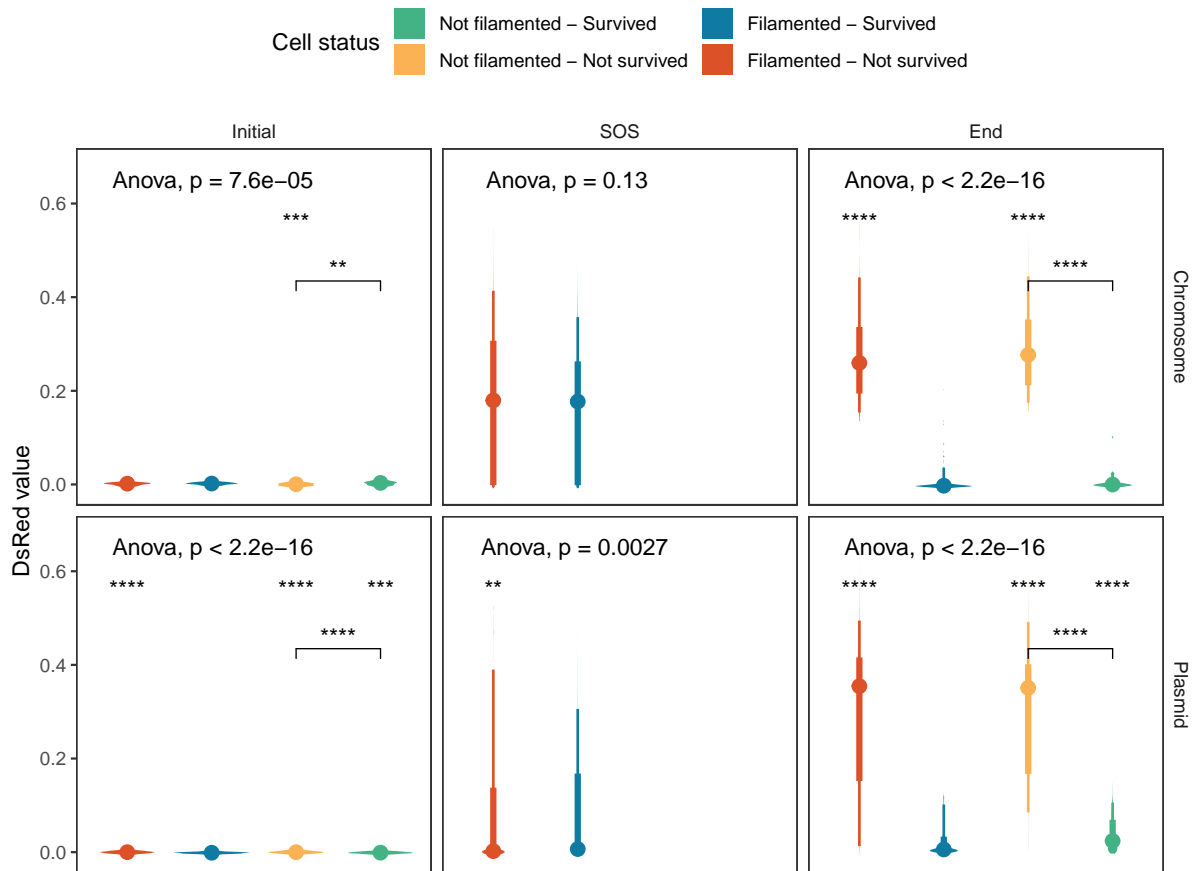


Figure 2.2: DsRed temporal distribution. To evaluate the incident effect of the antibiotic marked by DsRed on cells by class, we show its values at three key moments: start, filamentation (SOS), and end. The upper asterisks represent the significance value when comparing a group X to the filamented and surviving cell reference. Asterisks in a line indicate whether or not there is a significant difference in the survival of non-filamented cells. Dots represent the mean of each group. The line bars represents the distribution of the data. Although, at the initial time, we observe multiple significant differences, this is likely due to the intrinsic noise of the system since, as expected, the values are close to zero. We observed a difference between the surviving and non-filamented cells for the chromosomal strain for the SOS time, but the same did not occur for the plasmid strain. The final amount of DsRed makes a clear difference between survival and death.

On the other hand, GFP observations in Figure 2.3 showed us that filamented cells had low fluorescent intensities (low plasmid copy-number) at the beginning of the experiment.

In comparison, the chromosomal strain did not exhibit noticeable changes in GFP levels. For the final observation times, GFP measurements indicated that among the cells that did not filament, the ones that survived exhibited a reduced GFP expression concerning cells killed by the antibiotic. Meanwhile, for the filamented cells, whether surviving or dead, their GFP measurements indicated no difference at the beginning or the end of the experiment, suggesting the presence of other determinants of cell survival.

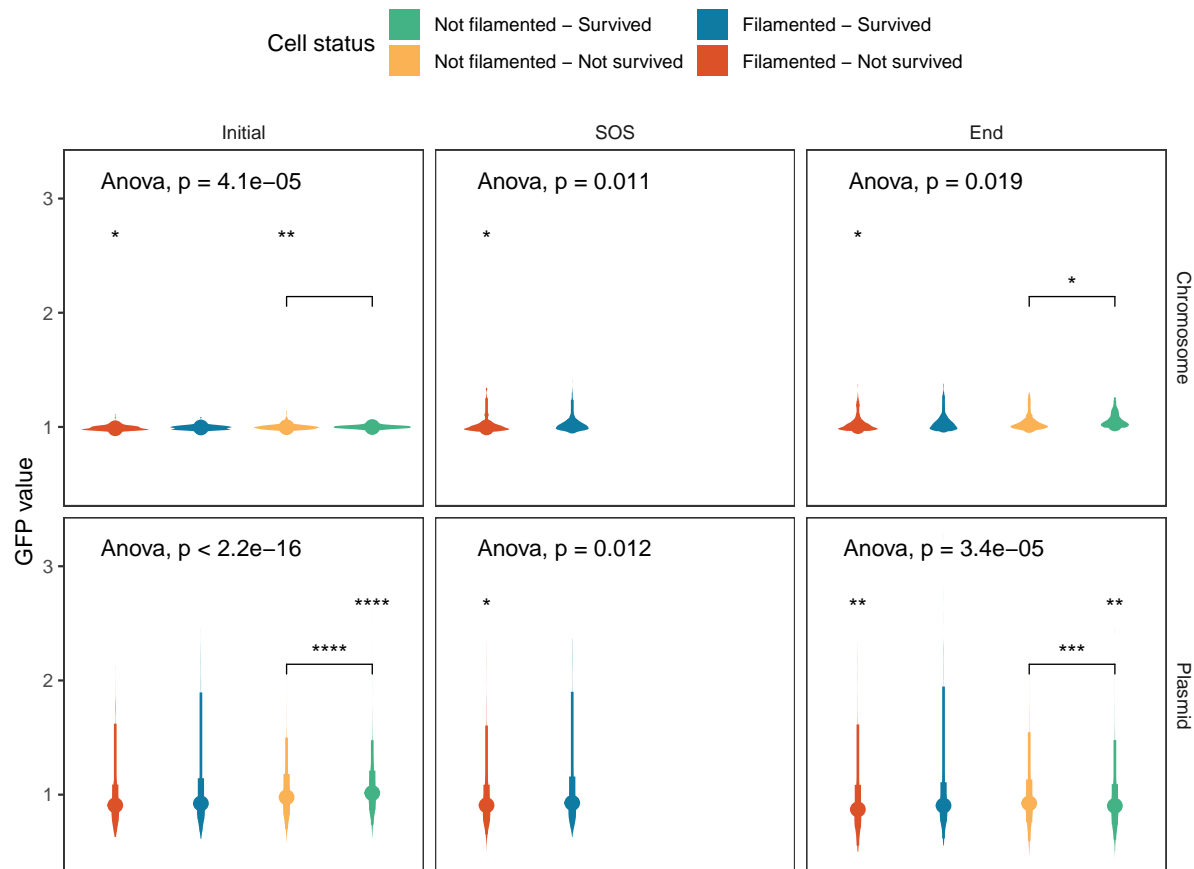


Figure 2.3: GFP temporal distribution. To evaluate the incident effect of the GFP on cells by class, we used the same notation as in Figure 2.2. The chromosomal strain exhibits variability in GFP at different time points, mainly due to experimental noise resulting from low fluorescent intensity values. As expected, filamented cells had a lower initial GFP in the plasmid strain. At the time of filamentation, there appear to be differences in fluorescence between surviving and dead cells. However, in the end time, we observed that the surviving non-filamented cells have lower GFP values than the non-filamented dead cells and alive filamented cells.

Cell length was one of the factors that GFP expression levels could not explain for cell survival. In Figure 2.4, we show that the conclusions regarding filamentation were applicable for both chromosomal and plasmid strains. For the initial times, filamented and survived cells were shorter in length than those that died but longer than not filamented cells of both classes, while non-filamented cells did not differ. We observed no length differences between cells at filamentation time. Thus, survival could depend on other factors, such as growth rate. In the final time, the results were well-defined. Surviving cells had a greater length than their non-surviving pair (*i.e.*, dead filamented and non-filamented cells). However, for filamented cells, surviving cells generally represent a distribution of higher final length values but are not as extensive as their dead counterpart. Which we could explain as a length limit to which cells can grow without dying. Nevertheless, we had no information to evaluate such a hypothesis.

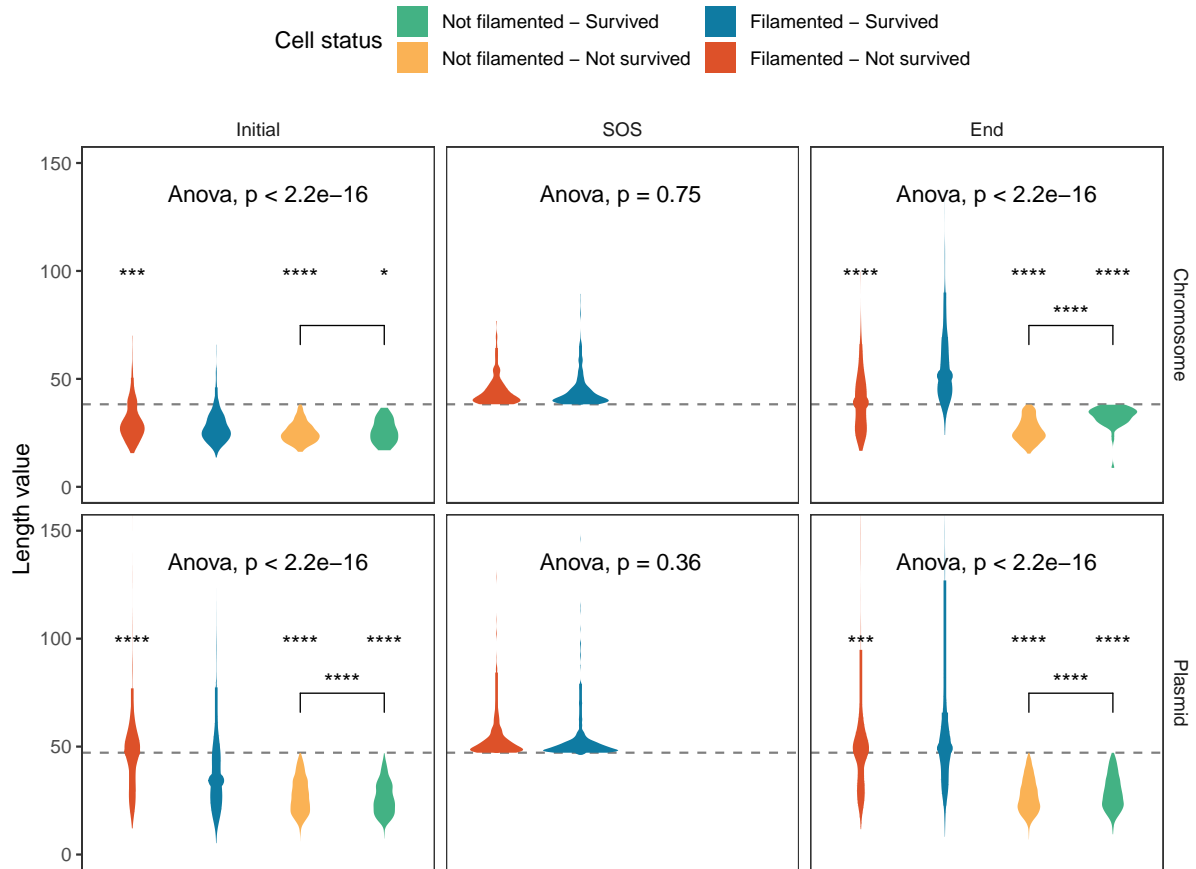


Figure 2.4: Length temporal distribution. To evaluate the incident effect of length on cells by class, we use the same notation as in Figure 2.2. The observations for both strains, chromosomal or plasmid, are the same. In the beginning, the surviving filamented cells already have a difference in length from the rest of the classes. At the time of filamentation, there is no difference to help determine whether the cell will survive or not. Finally, in the final time, it seems that the surviving filamented cells have a greater length than the rest of the groups. However, this length is moderate compared to the excess length shown by non-surviving filamented cells. On the other hand, we highlighted the growth of the surviving non-filamented cells. Therefore, although they did not reach a length for us to classify as filamented, the cells did resort to filamentation.

Once we observed the effects of GFP expression levels and lengths in determining whether a cell lives or dies, we projected the cells onto the plane. We painted them with their class status (See Figure 2.1) to determine whether these two variables contained the necessary

information to cluster the data correctly. In Figure 2.5, we show the initial GFP and length values projection. While, with some work, we could contextually place the results in Figure 2.3 and Figure 2.4, the initial values did not appear to determine the classes. Therefore, we explored the final versus initial values differences in Figure 2.6. With this new representation of the cells in the plane, we contextualized the statistical results presented in Figure 2.3 and Figure 2.4. Besides, it showed us that differences in length (*i.e.*, filamentation) and reductions in GFP expression are essential in determining cell survival. Though the clustering of cell status is not entirely separated, other variables affect the experimental results in cell survival.

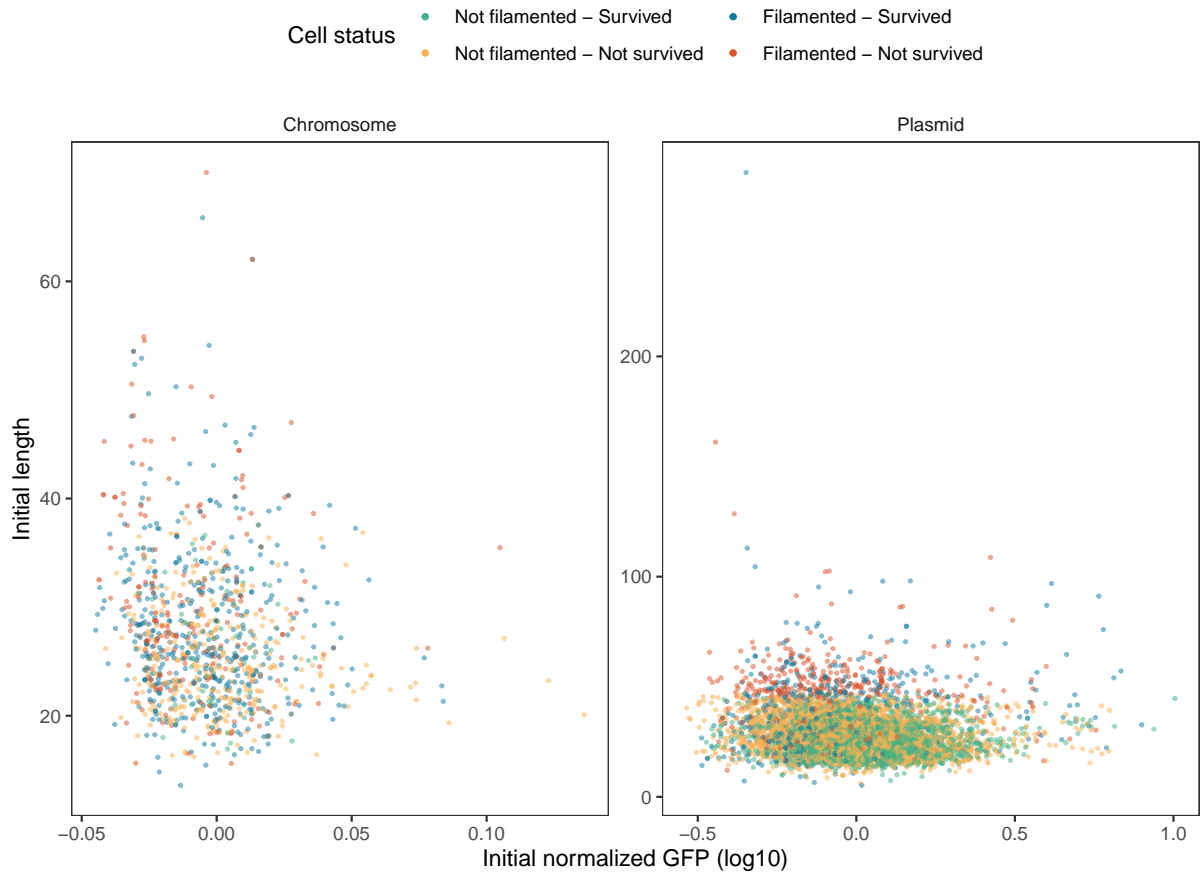


Figure 2.5: **Experiment's initial values.** By positioning a cell in space based on its initial length and GFP values, we can see that class separation occurs, but not as a strong signal. Therefore, we concluded that although the initial state influences the result, this is not everything. For this, we have the example of the length changes throughout the experiment caused by filamentation. In this graph, the GFP scale is at log10 to help us observe those minor differences between the experiments.

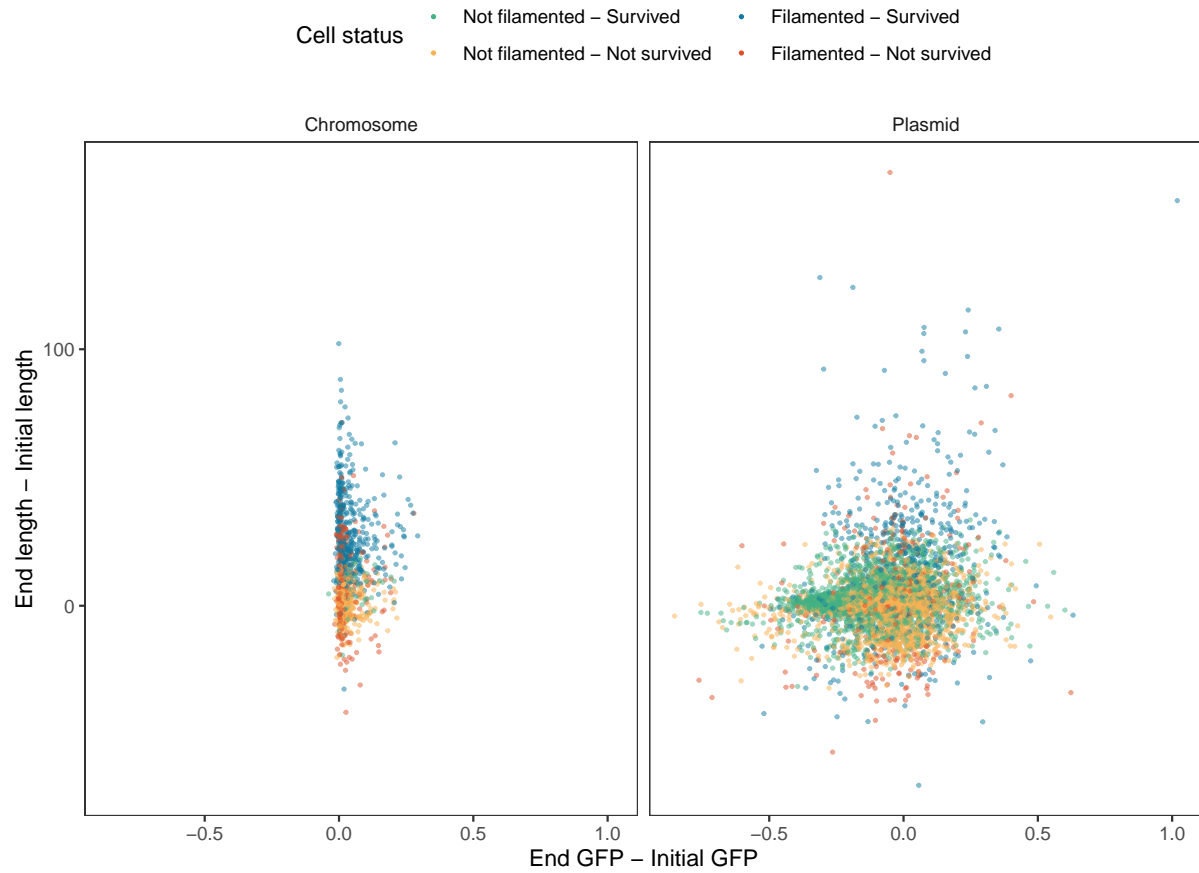


Figure 2.6: **Experiment's initial values differences.** By comparing the metric differences of the last observation and the first observation of a cell, we can separate mainly the surviving filamentoed cells from those that did not do it in both experiments (blue dots). Meanwhile, cells with plasmids form a small accumulation of surviving cells that did not produce filament (green dots). However, this has made a breakthrough in understanding what is affecting cell survival. There are still variables that we can include to understand this phenomenon better.

2.3.2 Number of divisions and cell age do not appear to play a clear role in determining cell survival

In Section 2.3.1, we explored the effect on cell survival through GFP variability and cell length. However, Figure 2.5 and Figure 2.6 showed us the possibility of other factors relevant to the phenomenon under study. As some papers in the literature suggest, some

of these other factors may be cell division and chronological age (*i.e.*, how much time has passed since the last cell division at the time of exposure to a toxic agent) (Moger-Reischer and Lennon 2019; Roostalu et al. 2008; Heinrich, Leslie, and Jonas 2015). Therefore, we chose to observe these two metrics in experiments at a purely qualitative level, *i.e.*, without the inclusion of, *e.g.*, metrics of membrane or cell cycle properties (Joseleau-Petit, Vinella, and D'Ari 1999).

Although we expected to see a small contribution, either by the number of divisions or cell age, in Figure 2.7 and Figure 2.8, we could not observe a precise effect of these variables on cell survival. Although they could have an explanation or biological significance, we decided to omit as relevant in the characterization of our cells, since the signal was not clear. However, we derived from this analysis a slightly simpler variable that tells us whether a cell underwent a cell division event or not. So it gives us a more generalized picture of the contribution of division to cell survival (see Figure 2.14).

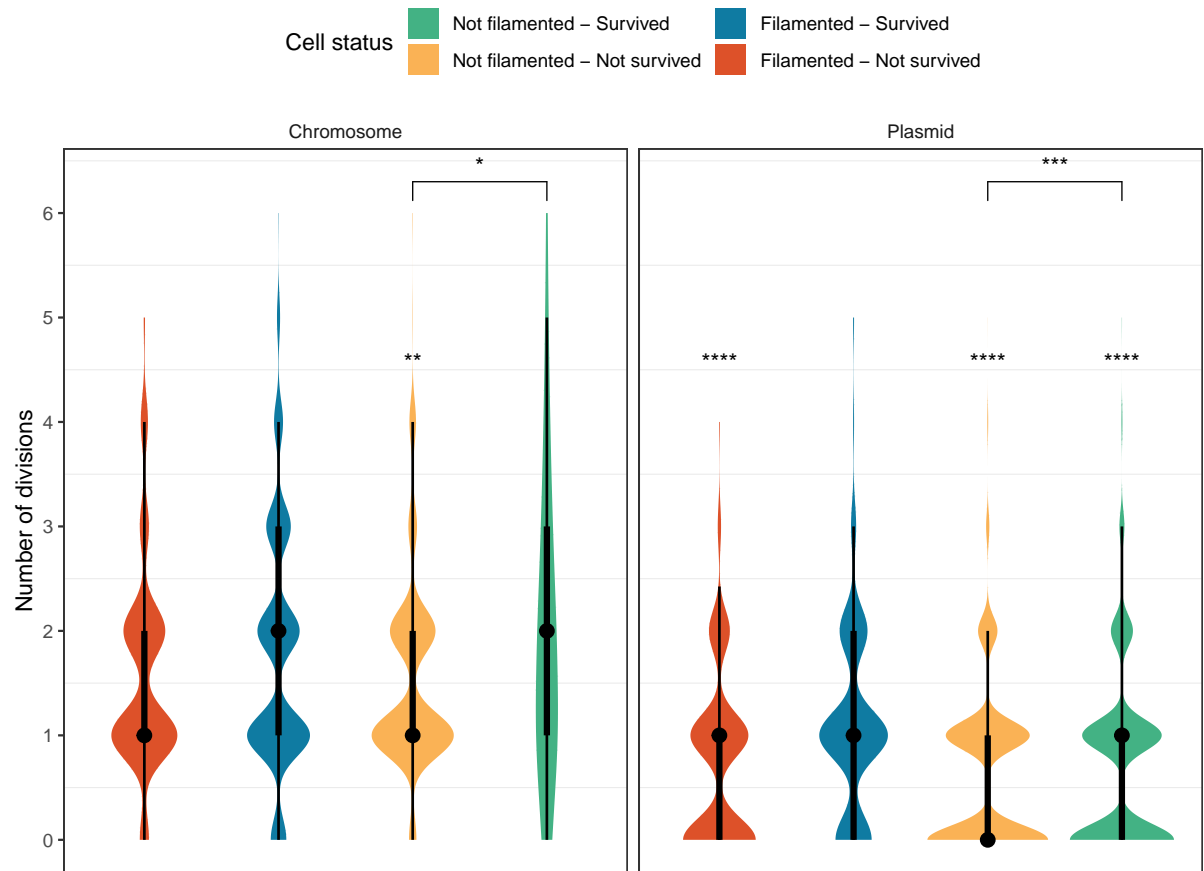


Figure 2.7: Cell's number of divisions. Both chromosomal and plasmid cells exhibited a wider distribution of divisions for the surviving cells against non-surviving cells. However, we did not appreciate a significant change between the chromosome filaments cells. Therefore, the number of cell divisions' contribution to filamentation remains uncertain.

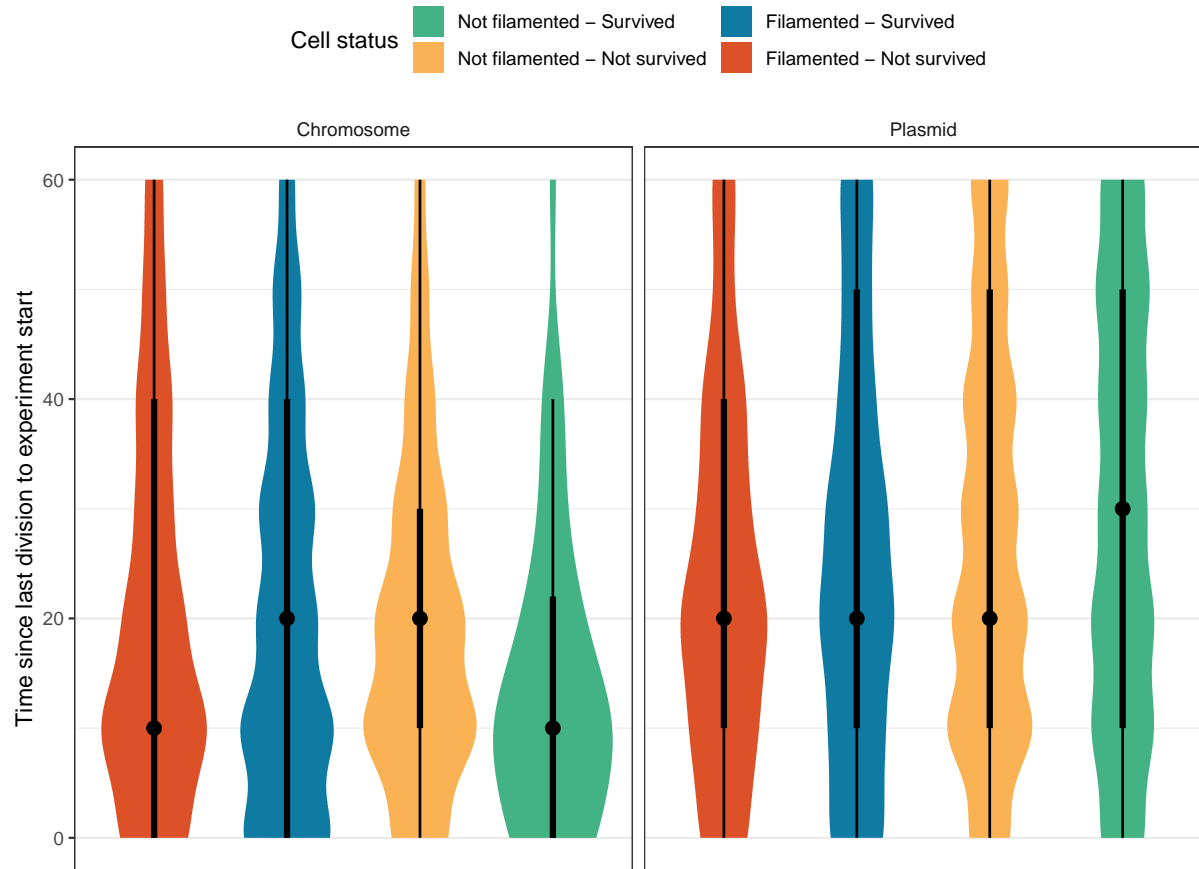


Figure 2.8: **Time elapsed since the last division at the beginning of the experiment.** The mean time of the last division before starting the experiment indicates that it did not influence the final result for chromosomal cells. There is a slight difference between the filamented-not survived cells and the rest for cells with plasmids. However, the signal does not appear to be strong on the survival role. Therefore, we conclude that we have no evidence to support that the time of the last division at the beginning of the experiment influences the final classification results.

2.3.3 Time to reach filamentation matters in determining cell survival

In Figure 2.2, Figure 2.3, and Figure 2.4, we showed how, at the time of filamentation, DsRed and GFP levels appeared indifferent to the cells. Therefore, we hypothesized that a possible variable determining cell survival could be its time to activate its anti-stress

response system that causes filamentation. Furthermore, we also guided our hypothesis by previous reports showing us how the gene expression level can induce filamentation with tight temporal coordination [x].

While, for our analyses, we did not measure the concentration of antibiotic that triggers filamentation per se, we indirectly quantified its effect by using the time it took for a cell to reach a length at which it is already considered a filamentating cell. Furthermore, to recognize that the observed effect was a product of the experiment, we decided to keep only filamented cells just once antibiotic exposure began.

Figure 2.9 shows how filamentation times are narrower for chromosomal cells than for plasmid-bearing cells. Then, we hypothesize that the effect could come from the heterogeneity in the plasmid copy number in the population. Also, interestingly, we observed that, for both experiments, cells that survived had longer filamentation times than those that died. These differences in response times suggest the following: 1) if the cell grows too fast, it will reach a limit and start to accumulate antibiotics constantly, and 2) if the cell grows too fast, likely, the cost of maintaining an ample length for prolonged periods of exposure will become counterproductive.

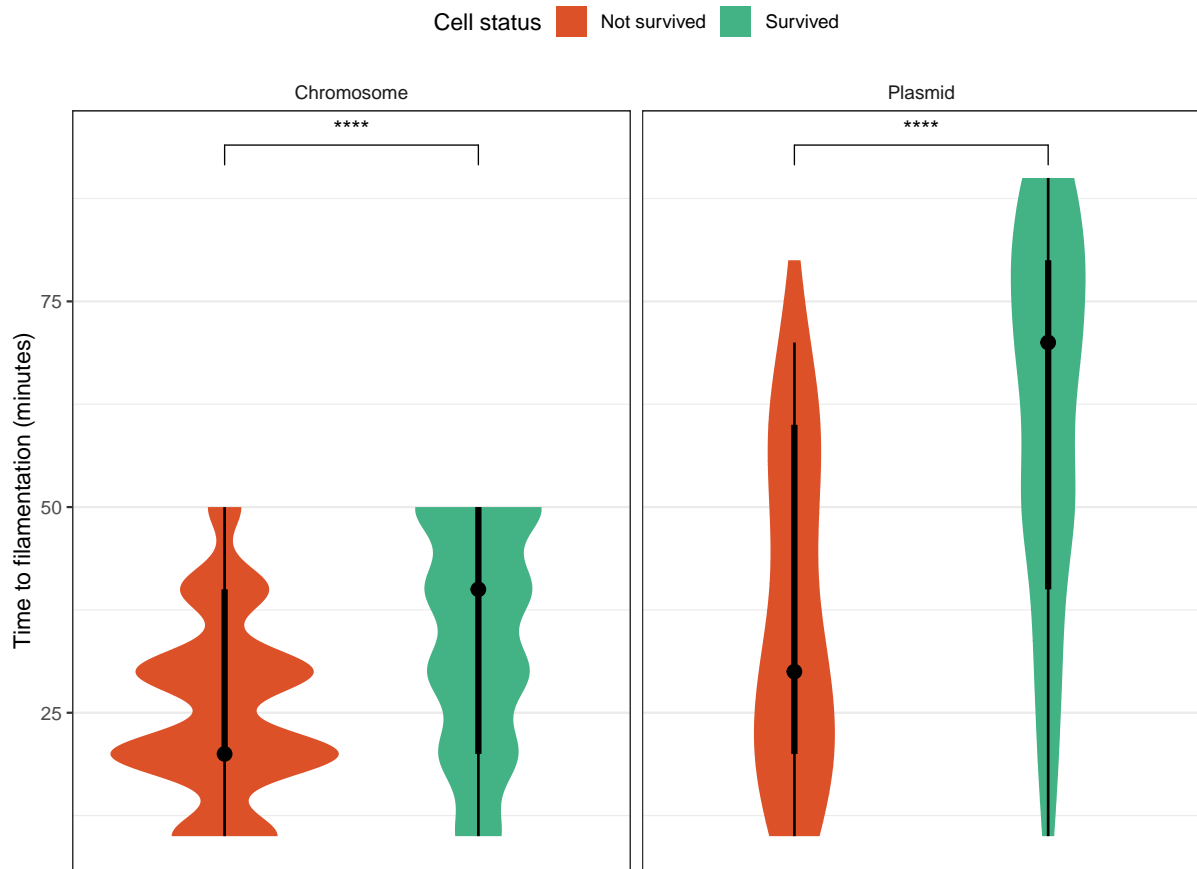


Figure 2.9: **Time to filamentation filtered.** We only keep cells that filamented during the antibiotic exposure to quantify their time to filamentation and its effect on survival. In this way, we normalize the start times for the calculation of the filamentation time. For both strains, the filamentation time had a more significant delay in the surviving cells.

In Figure Figure 2.10, we decided to project the results of Figure Figure 2.9 in a space similar to the one described in Figure Figure 2.5). Thus, we separated our data into cells that survived and cells that did not and painted them when it took them to reach their filamented state. We realized that, by adding this temporal component to the initial variables of length and GFP, we could separate surviving cells from dead cells to a greater degree. However, it may still not be enough, and there are still many other variables that play a crucial role in understanding the ecology of stress and how some cells will be survivors or not.

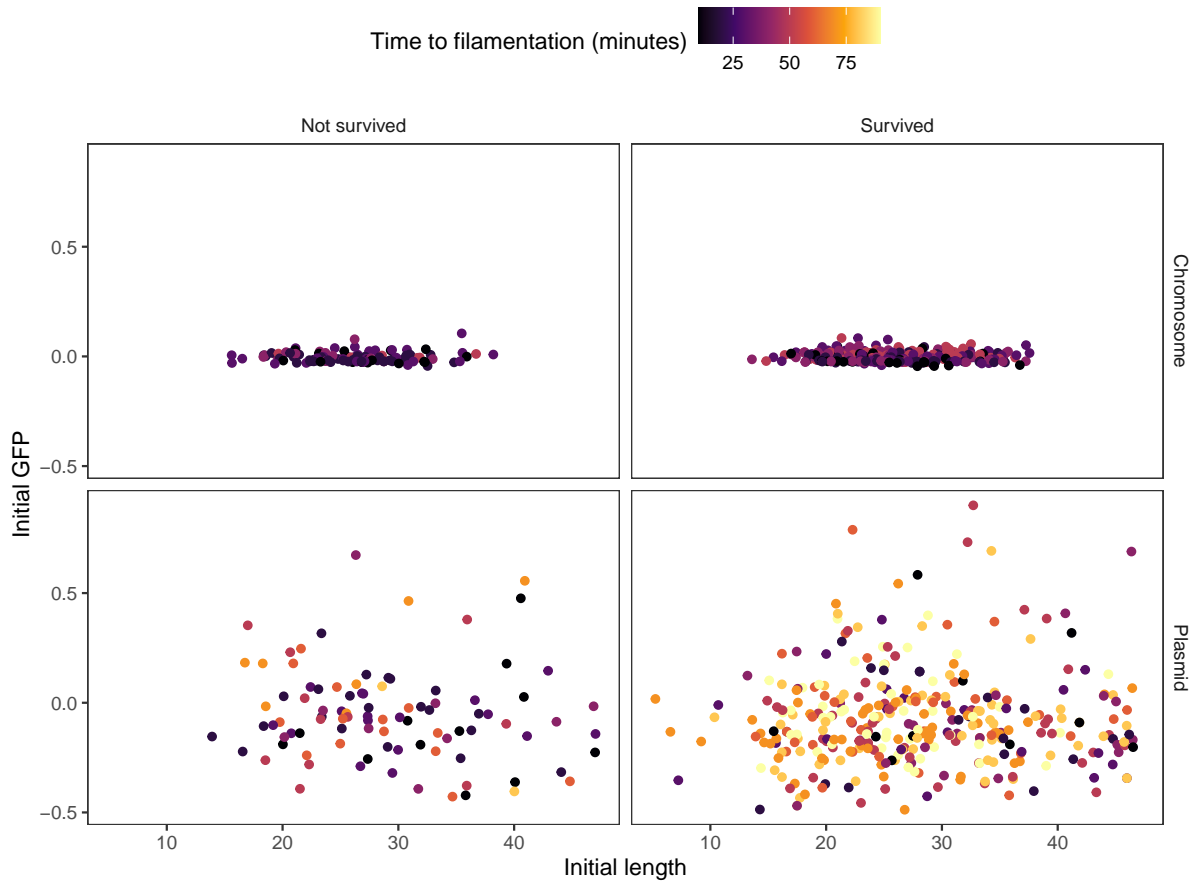


Figure 2.10: **Experiment initial values with time to filamentation.** As in Figure 2.5, including the time it will take for cells to filament allows us to better understand the phenomenon of survival. Cells that filamentoed and survived generally have a much higher delay than their non-filamented peers for both strains (see Figure 2.9).

2.3.4 Increasing the complexity of the system and analyzing it in an unsupervised way allows a correct classification of cell states

In the experiments, we observed the importance of GFP filamentation and variability for cell survival. Similarly, we realized that other variables must be affecting the final results. Filamentation and GFP variability alone did not fully recapitulate the expected behavior of the data. That is, the target variables did not capture the heterogeneity of the system.

The inability to reproduce cell classification led us to question two things: 1) the possibility that our sorting was wrong beforehand and 2) we did not have enough variables to capture the study phenomenon. We decided to take the unsupervised learning way to answer these subjects because it allows us to project our data without *a priori* knowledge.

We opted for the path of dimensionality reduction techniques where each variable or feature is equivalent to one dimension. The essence of dimensionality reduction is that it is not feasible to analyze each dimension with many dimensions. Furthermore, dimensionality reduction helps us counteract several problems such as reducing the complexity of a model, reducing the possibility of overfitting a model, removing all correlated variables, and, of course, visualizing our data in a two- or three-dimensional space for better appreciation. Improved visualization and identification of essential variables are the main reasons to guide and complement our research with this technique.

2.3.4.1 Principal Component Analysis (PCA) emphasizes the importance of cell length and its GFP in cell survival

The first dimensionality reduction technique we decided to use was Principal Component Analysis (PCA) ([Pearson 1901](#); [Hotelling 1936](#)). Scientist mainly uses PCA to create predictive models or in Exploratory Data Analysis (EDA). In our case, we only use it as an EDA.

For chromosomal and plasmid strain, in Figure [2.11](#) and Figure [2.12](#), we show the projection of the first two principal components (PCs), respectively. Figure [2.11](#) separates the manually annotated classes, surviving cells separated from non-surviving cells. However, for Figure [2.12](#), the class separation was a bit rougher but allowed us to separate the surviving filament cells from the dead ones.

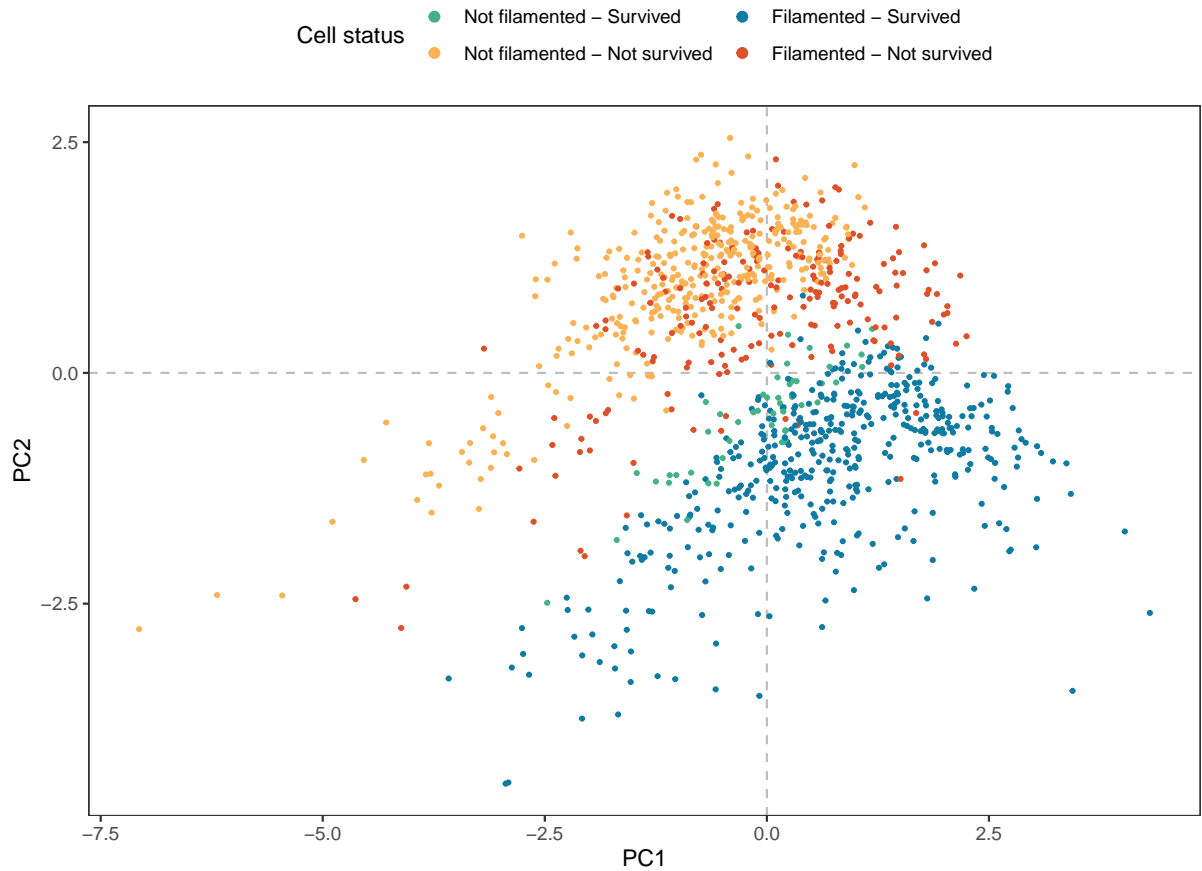


Figure 2.11: Principal Component Analysis of chromosomal strain. When integrating the information of different variables in a dimensionality reduction analysis, we observed a clear separation between the surviving cells and those that did not. The contributions that determined this phenomenon come mainly from the last amount of DsRed, GFP, and cell length (see Figure 2.13). Although it seems obvious, it effectively confirms that the temporal classification that we carry out makes sense. Longer length represents a greater uptake of antibiotics but in a much larger volume, so the net effect is an internal reduction of antibiotics (see Figure 3.1).

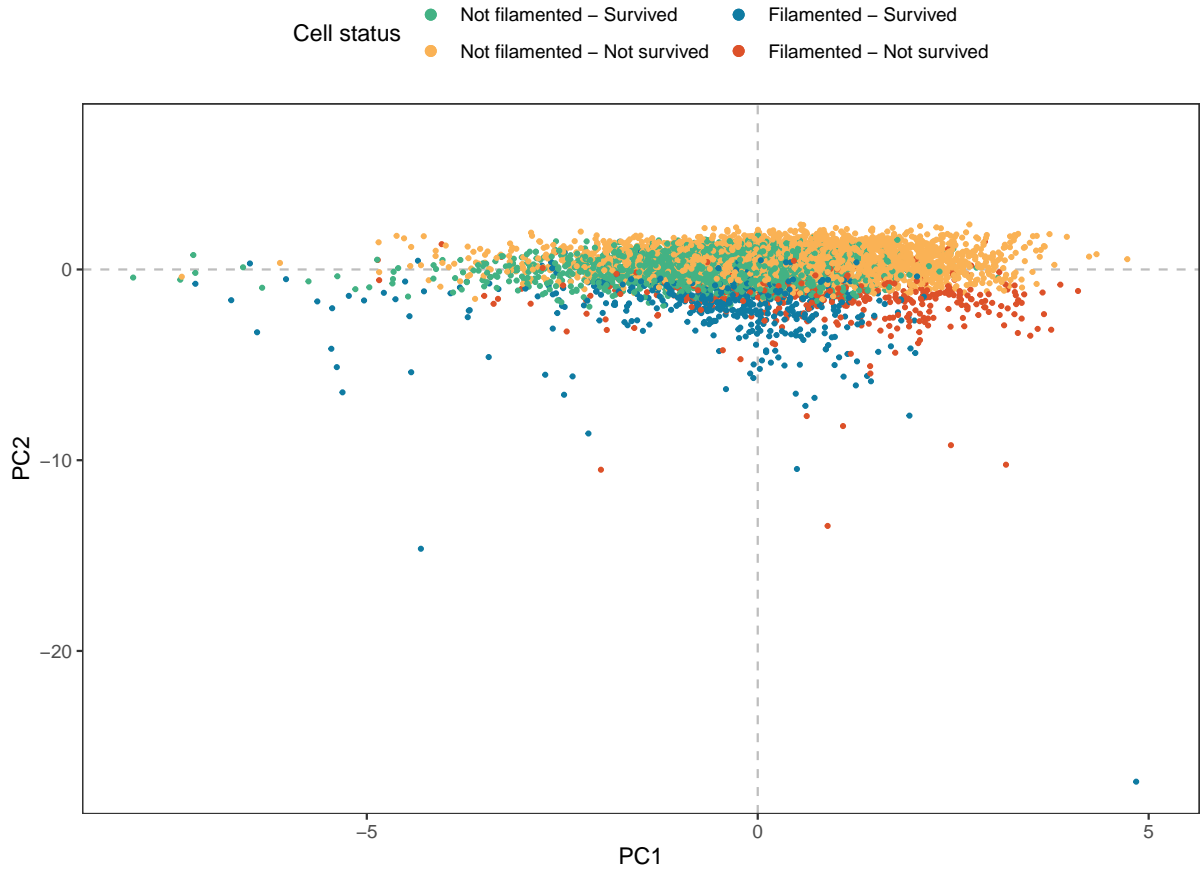


Figure 2.12: Principal Component Analysis of plasmid strain. By integrating the information from different variables in a dimensionality reduction analysis, we observed a clear separation between the filamented and non-filamented cells. Said class separation is given by component 2 (Y-axis), which is determined primarily by the initial and final lengths of the cells (see Figure 2.14). Furthermore, the classification also allows us to separate those filamented cells that died from those that survived. Therefore, despite the increase in the system's complexity, length plays a role in determining survival.

For their part, in Figure 2.13 and Figure 2.14, we show the total contribution of each variable per PC for the chromosomal and plasmid strain, respectively. Finding that, indeed, filamentation plays a crucial role in determining cell survival. For example, for PC2, we appreciated how the variable end DsRed directed the dots to the positive side, while the variable end and start length directed the dots to the opposing side. Therefore, we can support that filamentation has a role in moving cells away from having higher amounts of DsRed.

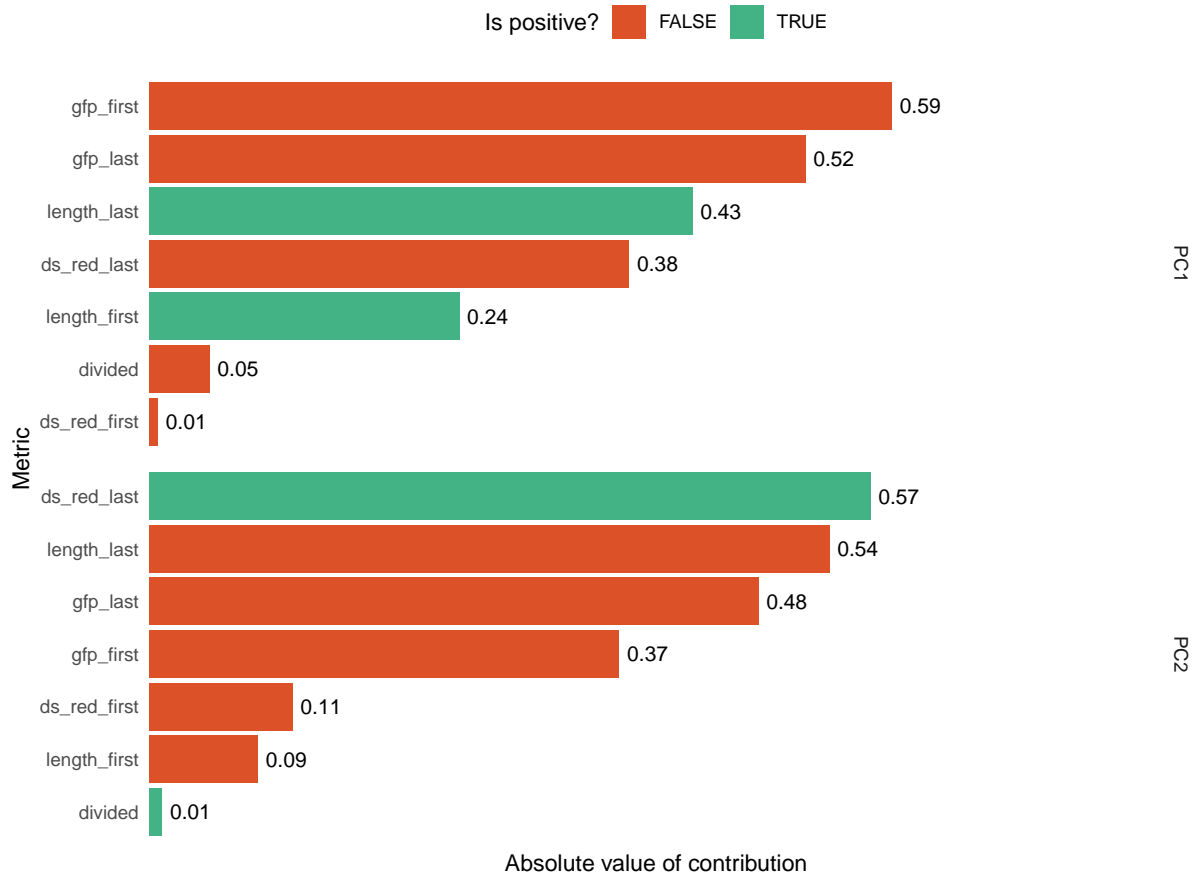


Figure 2.13: **Variables contribution of Principal Component Analysis of chromosomal strain.** In the Figure 2.11, we see that the classes we created manually reflected what we observed when performing a reduction of dimensions analysis. Here we show the individual contribution of each variable for the first two components. The variables that most affected components 1 and 2 (X-axis and Y-axis, respectively) are the final measurements of DsRed, GFP, length, and the initial amount of GFP. Given that they are chromosomal strains, we should note that this variability could be produced by intrinsic experimental noise that we could not remove. With that in mind, having the DsRed and the final length highlights the inherent role of cells by having increased its size.

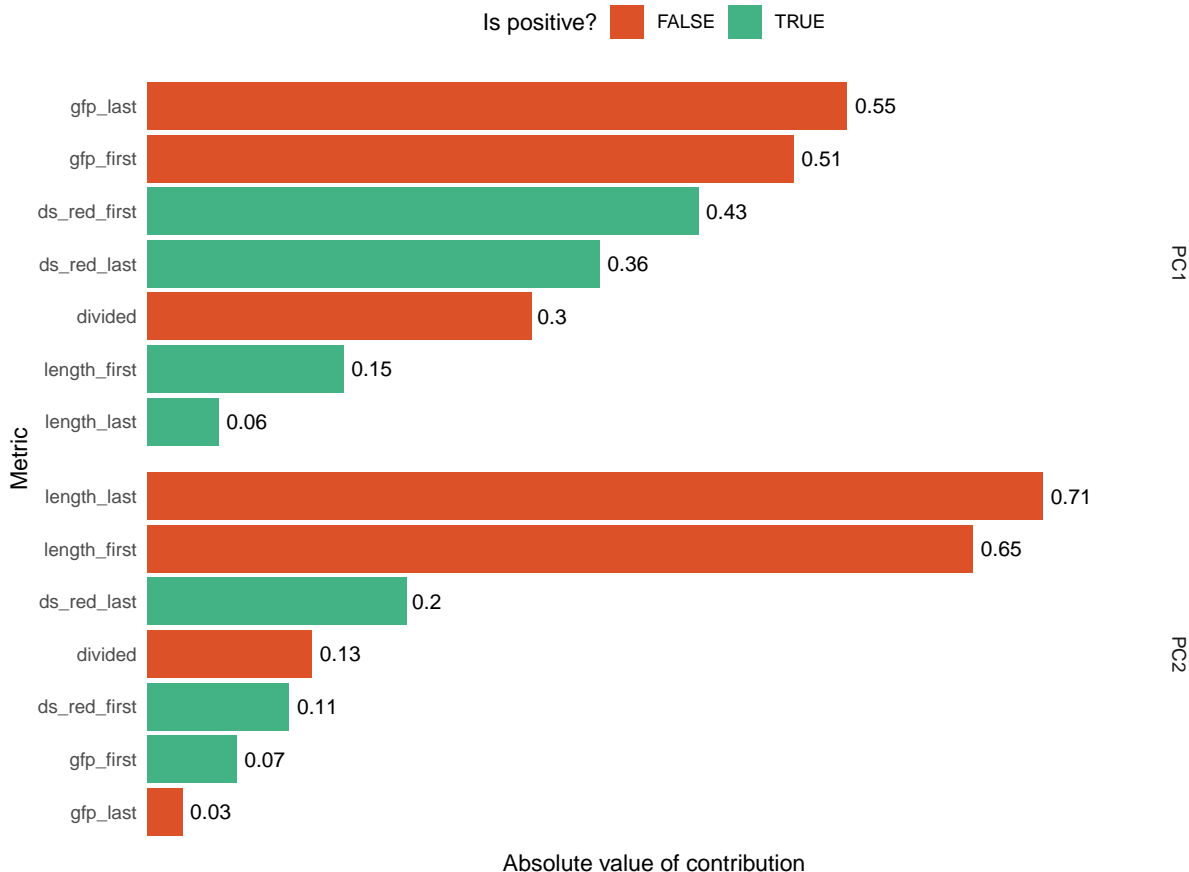


Figure 2.14: Variables contribution of Principal Component Analysis of plasmid strain. In Figure 2.12, we saw that we could separate the filamented cells from the non-filamented ones. The reduction analysis also shows a slight difference between surviving and dead cells within the small group of filamented cells. Here we offer the individual contribution of each variable for the first two components. For the first component (x-axis in Figure 2.11), the initial and final GFP measurements received mainly the variability. We expected this component's importance since, being a chromosomal strain, we hope that its inherent variation will be inherited into the system. On the other hand, the second component (Y-axis in Figure 2.11) was determined by the length of the cell. Factors that, in the chromosomal strain (see Figure 2.13), determined with the help of DsRed the separation between surviving and dead cells.

2.3.4.2 Uniform Manifold Approximation and Projection (UMAP) correctly represents the local structure of cell states

Staying with only a one-dimensionality reduction technique was not an option, so we used the UMAP technique ([McInnes, Healy, and Melville 2018](#)). We mainly decided to use UMAP for clustering purposes and see if the annotated clusters corresponded to the manually annotated ones. UMAP has certain advantages for these purposes, e.g., it preserves the global structure across the whole space, so the distances between clusters matter.

In Figure [2.15](#) and Figure [2.16](#), we show how, using the same variables used in the “PCA” section, UMAP was able to cluster the four proposed classes correctly. Interestingly, in Figure [2.15](#), UMAP formed three general groups and four for Figure [2.16](#). However, in general, UMAP clustered the surviving cells from those that did not survived. On investigating why this separation occurred, we found that the large groups coalesced into one another if we eliminated the division variable. So, in a way, the division also has a role in determining survival, but it is not essential or at least not over-represented in our data.

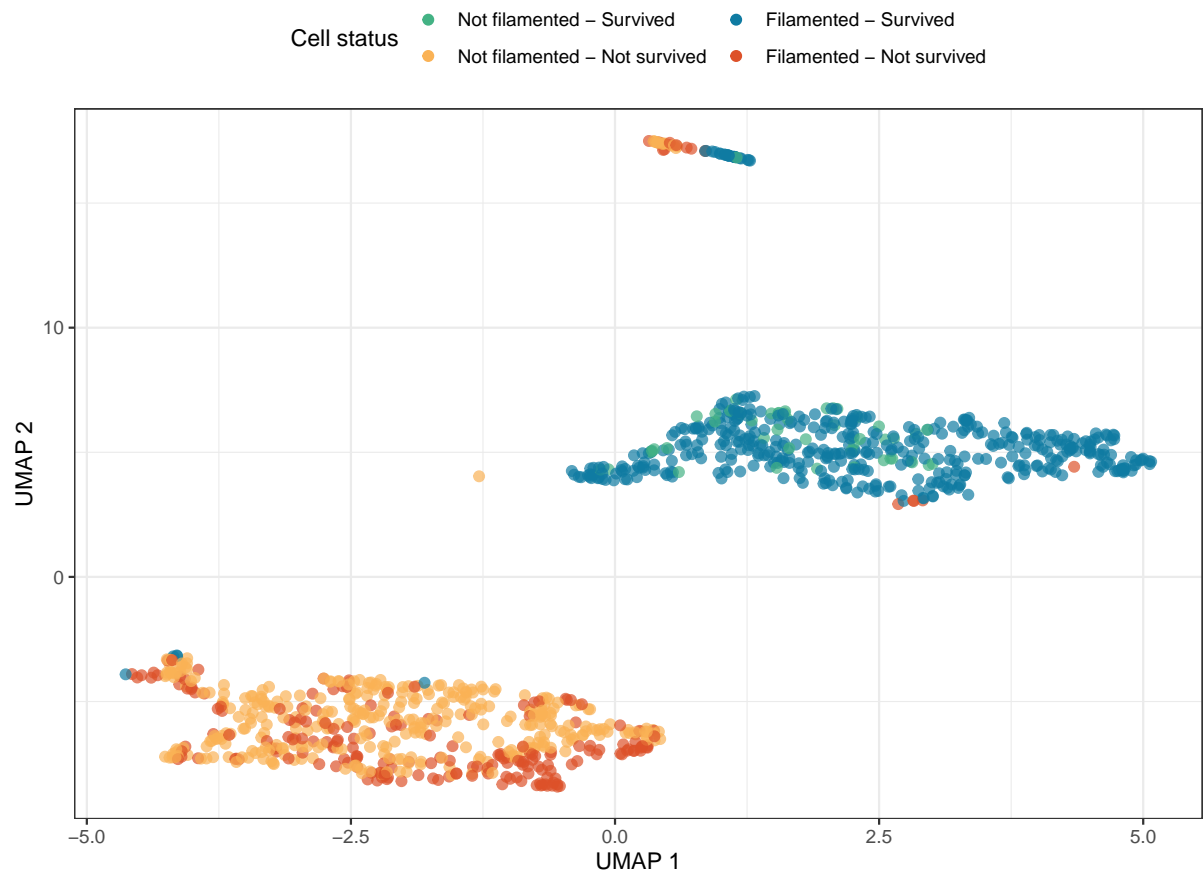


Figure 2.15: **UMAP coordinates of chromosome strain.** We represented the cells in a low dimensional space. This new projection made it possible to group the cells that survived and those that did not. Therefore, as in PCA Figure 2.11, this technique supports the manual classification that we carry out.

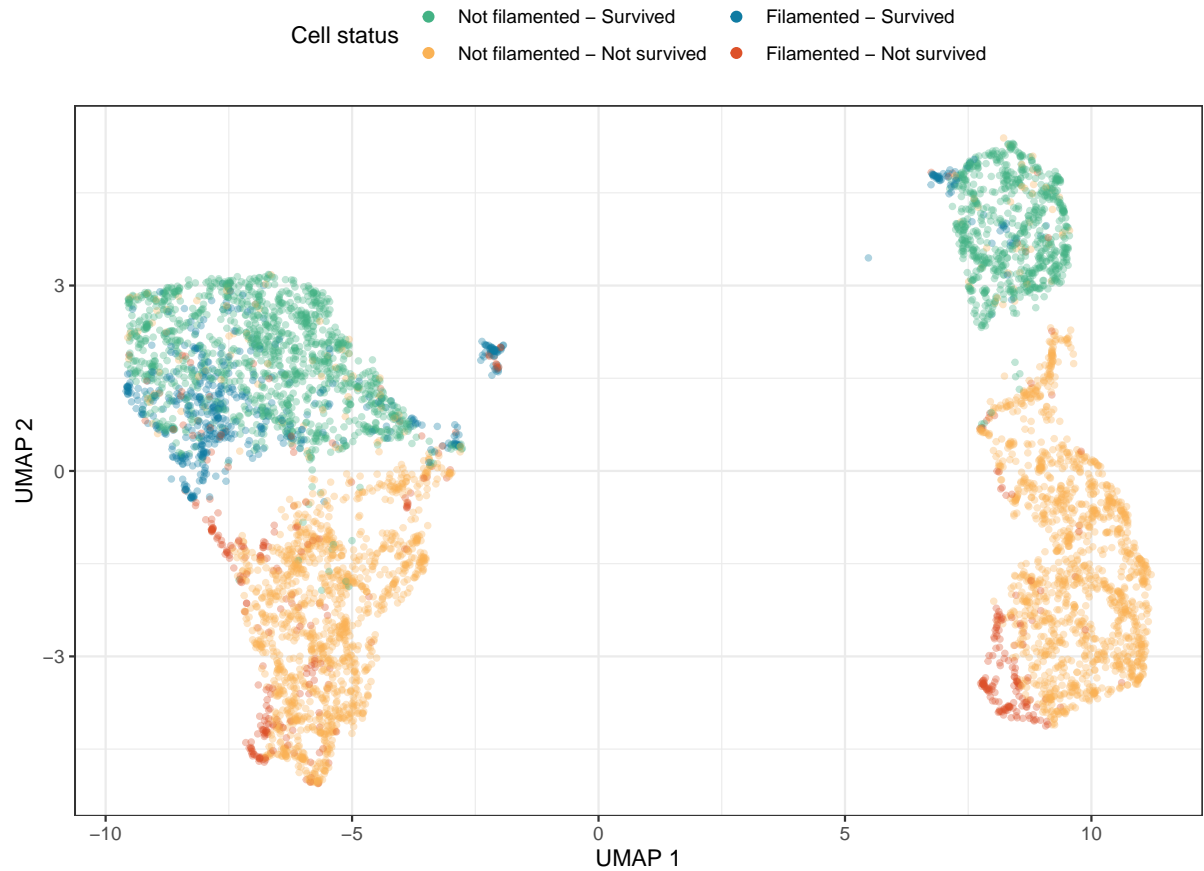


Figure 2.16: **UMAP coordinates of plasmid strain.** As in its Figure 2.15 pair, the representation in a low-dimensional space helped classify the cells, grouping mainly into four groups, two of survivors and two of non-survivors. The variable *division* marks the separation of classes. The *division* variable indicates whether a cell is divided during its lifetime or not. Together, the UMAP represents the manually assigned classes.

2.3.5 Population dynamics reveal how filamentation contributes cell survival

From the full tracking dataset, we evaluated how the different cell states behaved over time—for example, understanding how the cells absorbed antibiotics or how they elongated in time. In contrast to the dataset generated in the Section 2.3.1, we did not truncate the results 10 minutes after the antibiotic exposure. In this way, we were able to observe cell behavior before and after the presence of the toxic agent.

In Figure 2.17, we observed a small fraction of cells that were already filamentous without exposure to the toxic agent in both cell strains. However, after the onset of antibiotic exposure at minute 60, we observed increases in the proportion of filamented cells. It is interesting to note how filamented cells grew after antibiotic exposure for the chromosomal strain. We speculate that this post-antibiotic growth exists because, once the SOS system that triggers filamentation is activated, the system continues to grow until it reaches a limit regardless of whether the damaging agent is still present or not (Sheryl S. Justice et al. 2008; Mückl et al. 2018). Moreover, we observed how the cells start to divide again after some time because the proportion of non-filament cells starts to grow while the filament cells start to divide. We observed the same effects for the plasmid strain. However, by experimental design, the number of filament cells expected was much lower.

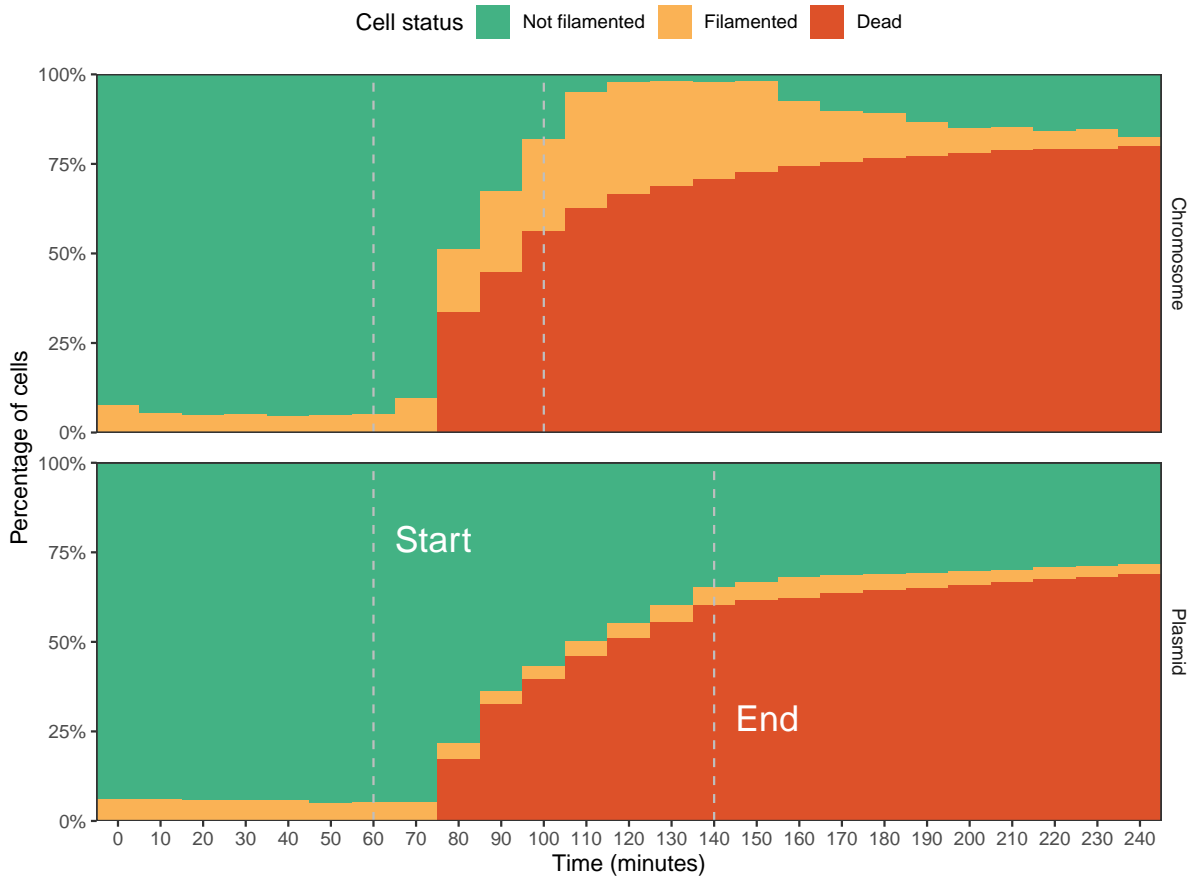


Figure 2.17: Population status over time. We calculate how many cells of each type existed for each time point: non-filamented and filamented living cells (blue and green areas, respectively) and dead cells (red area; we considered *dead* cells as those cells that existed at one time and then stopped tracking). The black vertical lines represent the start and end of antibiotic exposure for each experiment. The effect of filamentation and its spread after exposure to the antibiotic is evident for the chromosomal strain. The experiment was finalized with the resolution of the cells when they returned to their non-filamented state. For its part, for the plasmid strain, it is observed how the filamented cells begin to appear slowly. Their proportion is as expected, given that the population had a wide distribution of GFP that allowed them to combat exposure to the antibiotic.

In Figure 2.18, we showed how once antibiotics exposure began, those cells that died had a much faster increase in DsRed than those that did manage to live, regardless of whether they filamented or not. On the other hand, surviving cells managed to maintain their

DsRed levels relatively stable. We noted that length was critical for the surviving cells for the chromosomal strain by turning to the GFP and length variables for a temporal explanation. Even cells categorized as non-filamented reached the filamentation threshold minutes after antibiotic exposure. However, the distinction of live or dead filamented cells was not as evident as expected. As for cells with plasmids, the effect on GFP for surviving cells was maintained for filamented cells and decreased for non-filamented cells. For the filament cells that died, we showed that they had, on average, a much longer initial length than the surviving cells, so we also consider it as a necessary factor in understanding which variables affect cell survival.

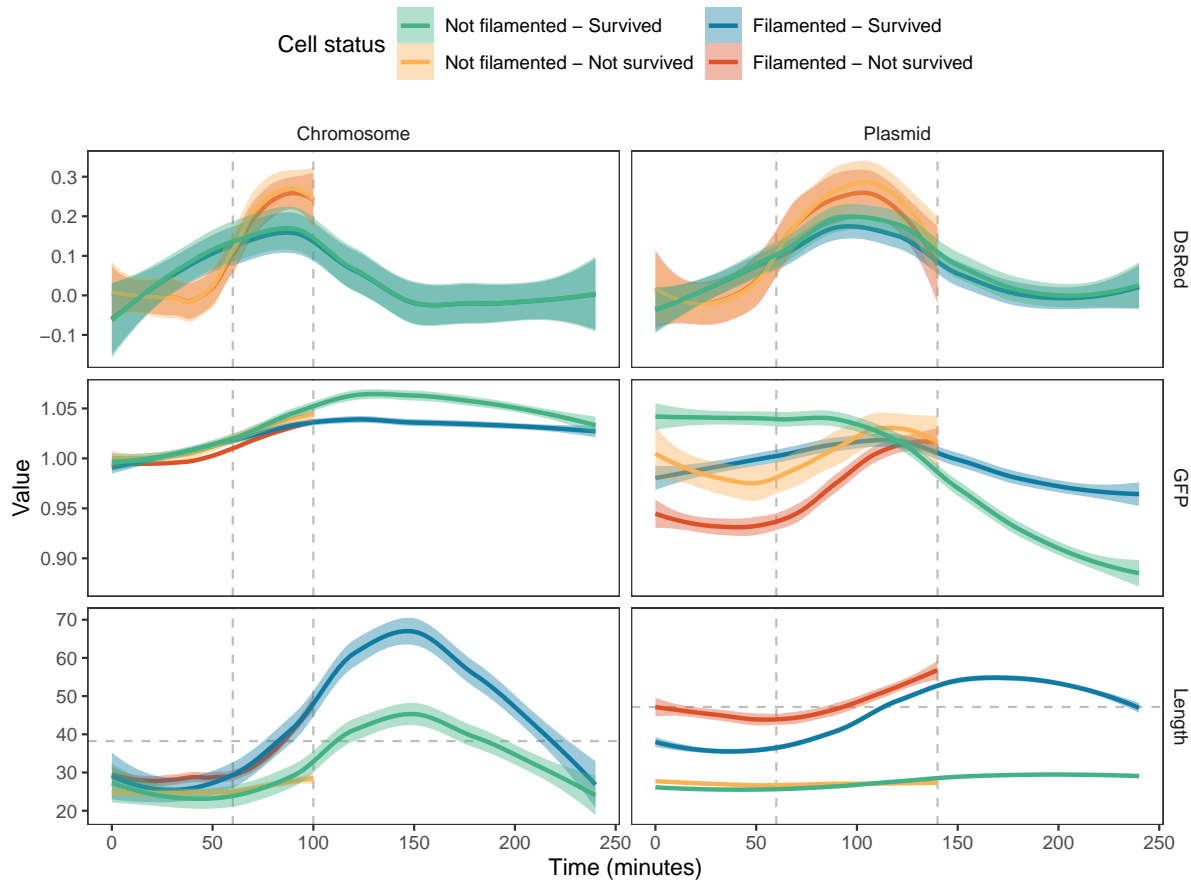


Figure 2.18: **Population measurements over time.** The colored lines symbolize the average value of each metric at each instant of time, while its surrounded gray shaded area represents the 95% confidence interval. The vertical lines represent the start and end of antibiotic exposure. The horizontal line in the length metric symbolizes the threshold to consider a cell filament. We observed a faster increase of DsRed for the non-surviving populations in both experiments. Regarding the GFP metric, the behavior is relatively stable for the chromosomal strain. In contrast, for the plasmid strain, a decline in GFP is observed for the population that did not survive. For the length metric, it is interesting to note how the chromosome cells that did not filament continued to grow past the filamentation threshold once the exposure to the antibiotic in the chromosomal strain had ended. On the other hand, the filamented and dead cells seem to have a greater length from the beginning for the plasmid strain.

2.3.6 Heterogeneity in plasmid copy-number allows various forms of survival in addition to filamentation

We are confident that filamentation has a fundamental role in determining cell survival, with what we have shown so far. However, for plasmid cells, we have a component that is of our complete interest; heterogeneity. Each cell can possess a different plasmid copy-number; thus, each could show a different behavior under stress ([San Millan et al. 2016](#)). For instance, heterogeneity can produce resistant cells that do not suffer damage, susceptible cells, and cells that form filaments to mitigate environmental stress.

To study the effect of variability in plasmid copy number in the survival probability of the population, we decided to group cells by the proportion of initial GFP with respect to the population maximum. We defined 100% of the population as the number of total cells at the onset of antibiotic exposure. Figure [2.19](#) shows how the cells with the highest amount of GFP remained unchanged once antibiotic exposure began, while the rest of the cells started to decrease their percentage of surviving cells. However, the decrease was not linear. On the contrary, we observed a bi-modal distribution on the reduction of live cells. An average GFP point provided higher survival than a point below or above the average (except for cells very close to the population maximum).

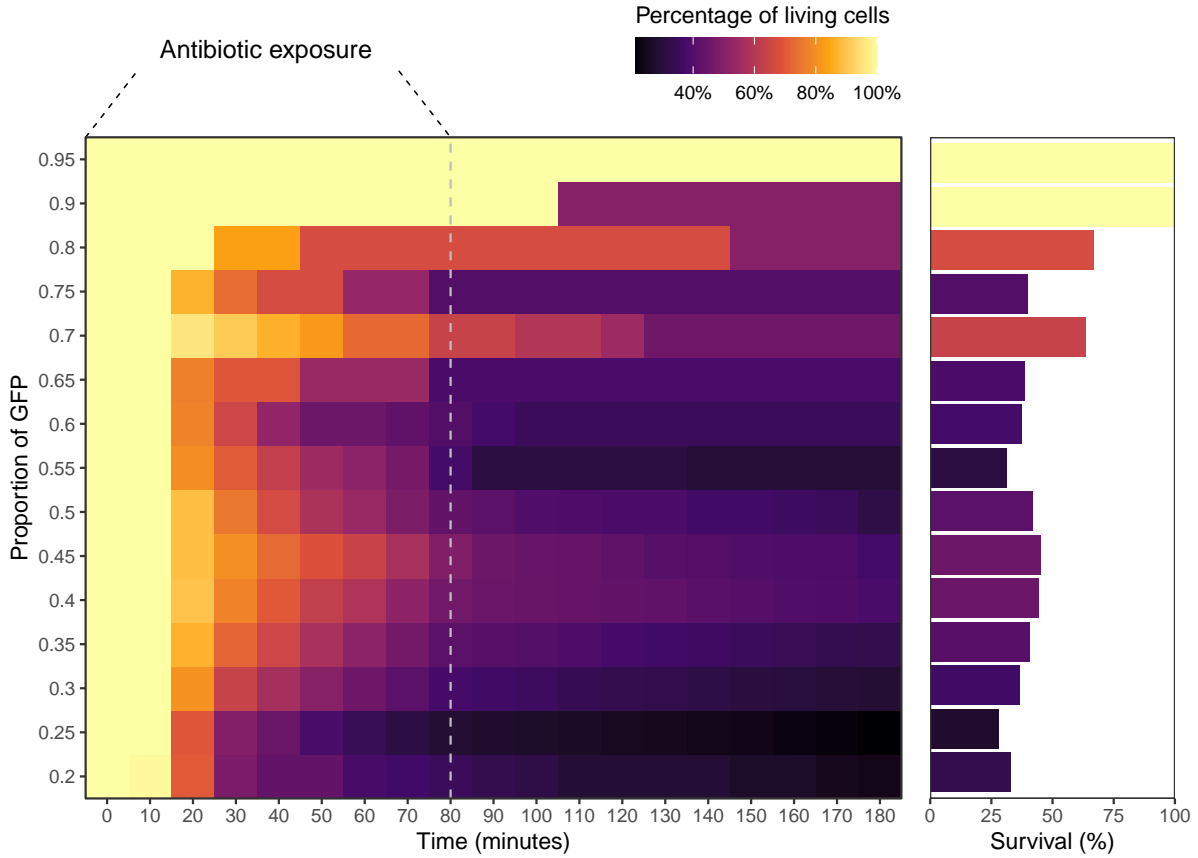


Figure 2.19: **Population survivals binned by initial GFP over time.** We categorized the cells' GFP into ranges of proportions 0.05 concerning the maximum amount of GFP in the population. 100% cells per bin of GFP was taken as the number of cells one frame before the start of exposure to the antibiotic (minute 50). Therefore, dark to light colors represent a generation of new cells, and light to dark colors the death of cells. The black vertical bars represent the start and end of the antibiotic exposure. Bars size and color on the right represent the percentage of the living cells 10 minutes after the end of the experiment. As shown in Figure 2.20, we showed that the surviving cells appear to follow something similar to a bimodal distribution. More cells survive with a moderate amount of GFP or with an amount close to the maximum of the population.

Therefore, what we observed was a bimodal distribution for GFP-dependent cell survival. In order to show this effect more clearly, in Figure 2.20, we plotted the survival probability for each GFP bin without normalizing for the population maximum. This new plot allowed

us to observe how the bimodal survival distribution occurs for cells that did not grow as filaments, whereas cells that filament increase their survival probability gradually as they have more initial GFP (see also Figure 2.3).-distribution).

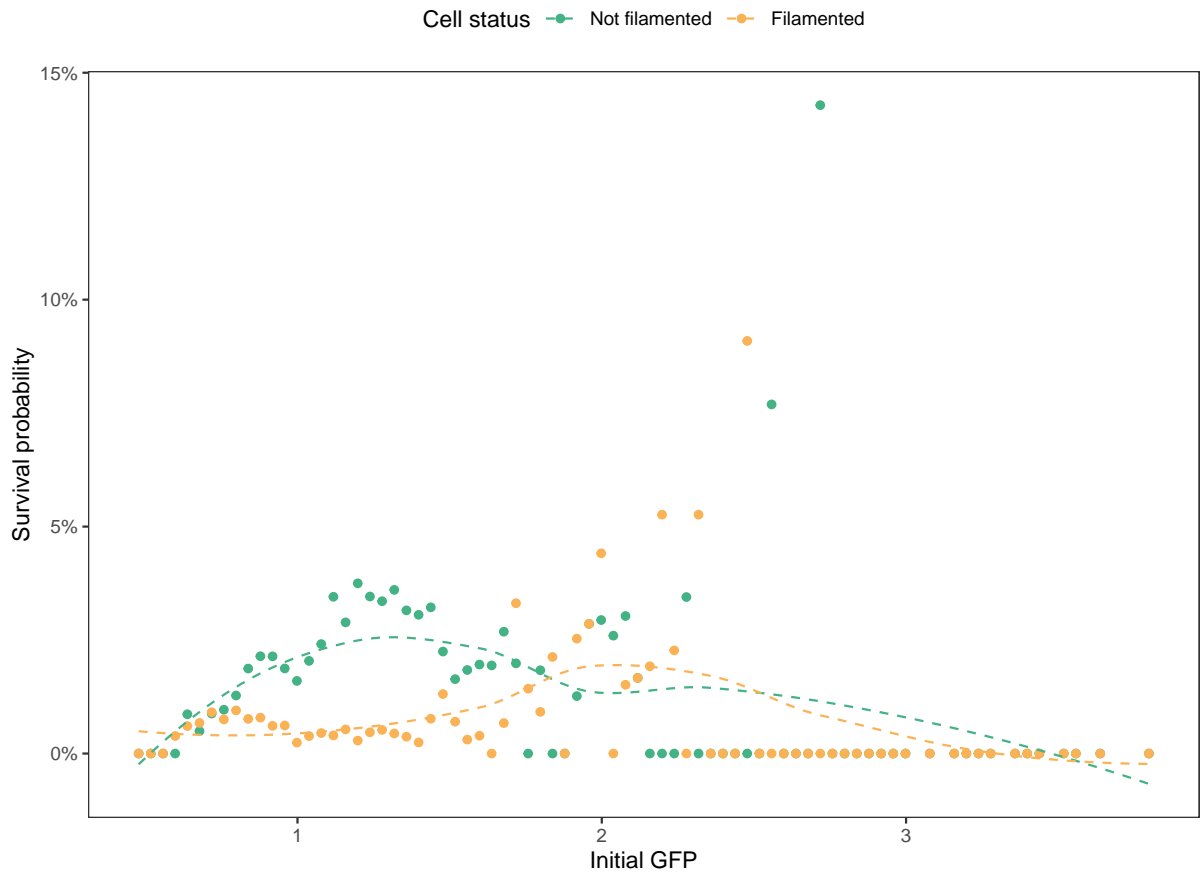


Figure 2.20: **Plasmid initial GFP survival probability.** We calculated the survival probability after comparing the population distributions of GFP with those of the cells that managed to survive. To assess survival by GFP, we only used plasmid cells. For non-filamented cells (blue dots), a bell forms with an upturned tail. On the other hand, for the filamented cells (red dots), a continuous increase in survival is shown just when it seems that the probability of the non-filamented cells has decreased. In global, much GFP has higher resistance, but an average GFP value without filamentation also increases the probability of survival.

As in Figure 2.20, in Figure 2.21, we show the survival probability given an initial length. We observe that survival is higher for cells that did not grow as filament if the initial

length was less than the average. In contrast, for filamented cells, the probability of survival increased as cells length was longer at the beginning of the experiment (see also Figure 2.4). However, it is noteworthy that the probability of survival had a limit in which a higher initial length meant a lower probability of survival (see red dotted lines in Figure 2.21).

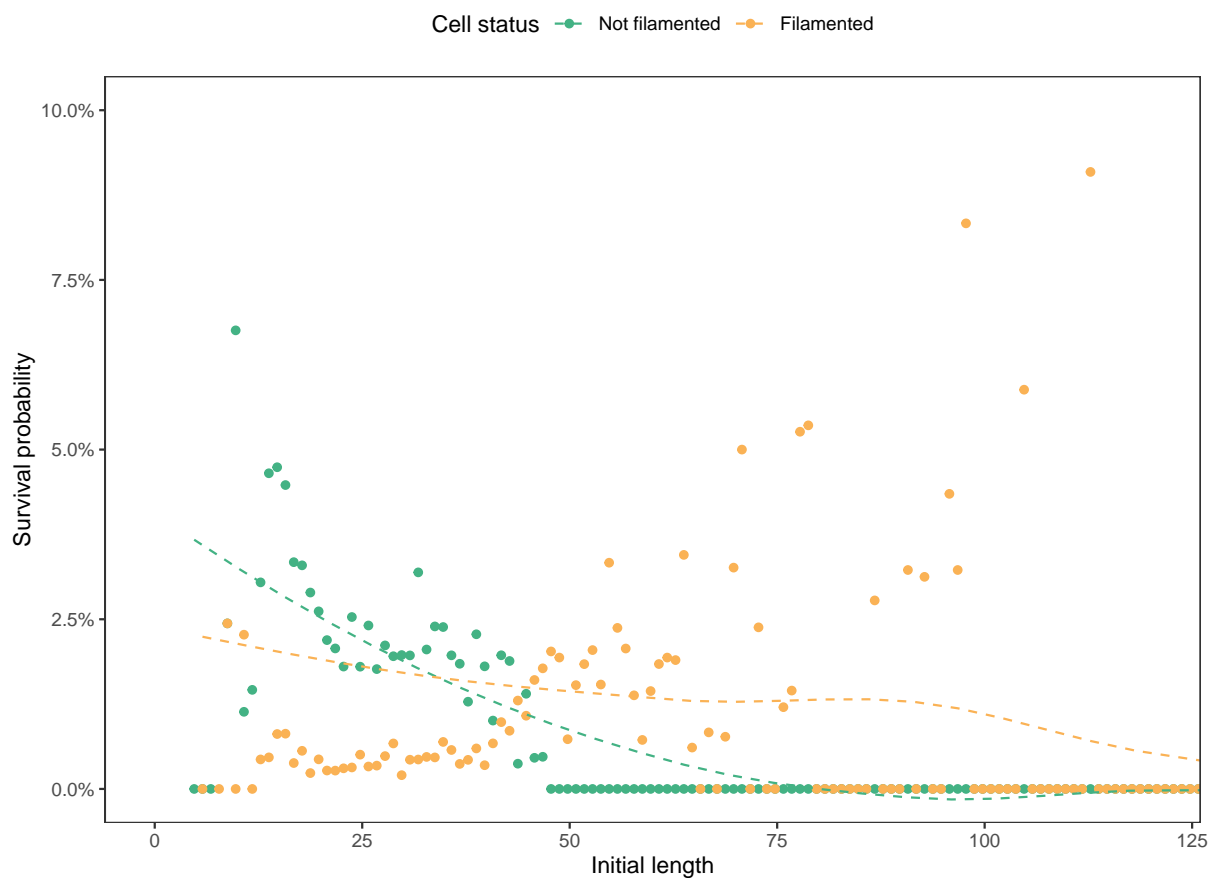


Figure 2.21: Plasmid initial length survival probability. We calculated the survival probability after comparing the population distributions of length with those of the cells that managed to survive. For non-filamented cells (blue dots), the survival probability is higher for those cells with small initial lengths, while it seems to decrease with a more extensive initial size. For their part, for filamented cells (red dots), the probability of survival increases according to their length but then declines when the cells are too long at first (see red dotted line). Therefore, in general, a small and moderate length or an initial length already filamented from the beginning increases the chances of survival.

2.4 Discussion

Here, we evaluated different variables that could determine cell survival upon exposure to toxic agents by studying two experimental populations of *E. coli*, one strain with a resistance gene on the chromosome and the other on multicopy plasmids. We identified two variables that are predominantly responsible for cell survival: cell length and GFP amount related to the cell's inherent resistance to the toxic agent and heterogeneity in response times.

On the other hand, as other studies have already mentioned ([Heinrich, Leslie, and Jonas 2015](#); [J. D. Wang and Levin 2009](#)), we examined cell activity and youth in a minimalistic way. While the distribution of the number of divisions exemplifies a broader and more uniform range for the surviving cells, the cells that died showed a tendency to a lower number of divisions. However, for the study of cellular youth at the time of exposure to the toxic agent, the results did not show a clear pattern of behavior for cell fate determination. Therefore, it would be interesting to study cellular youth at a higher level of complexity in future studies to understand its contribution to cell survival.

Interestingly, when we used temporal measurements of cell length, GFP, DsRed, and if a cell divided, we could recapitulate, for the most part, the fates of cellular states (see [Section 2.3.1](#) and [Section 2.3.4](#)). Thus, increasing the system's complexity led to better clustering cell states, but not how these factors interact biologically in determining cell survival. Therefore, we decided to postulate a mathematical model that helps us understand the critical components in cell survival.

3 Models to the rescue; filamentation abstraction

3.1 Introduction

By integrating information from the environment, cells can alter their cell cycle. For instance, some cells arrest the cell division in the presence of toxic agents but continue to grow. Previous studies have shown that this filamentation phenomenon provides a mechanism that enables cells to cope with stress, which leads to an increase in the probability of survival ([Sheryl S. Justice et al. 2008](#)). For example, filamentation can be a process capable of subverting innate defenses during urinary tract infection, facilitating the transition of additional rounds of intracellular bacterial community formation ([S. S. Justice et al. 2006](#)).

Although filament growth can help mitigate environmental stress (e.g., by activating the SOS response system ([Sheryl S. Justice et al. 2008](#))), the evolutionary benefits of producing elongated cells that do not divide are unclear. Here, we proposed a mathematical model based on ordinary differential equations that explicitly considers the concentration of intracellular toxin as a function of the cell's length (see [Equation 3.1](#)). The model is built based on the growth ratio of measurements of the surface area (SA) and the cell volume (V), whereby the uptake rate of the toxin depends on the SA . However, V 's rate of change for SA is higher than SA for V , which results in a transient reduction in the intracellular toxin concentration (see [Figure 3.1](#))). Therefore, we hypothesized that this geometric interpretation of filamentation represents a biophysical defense line to increase the probability of a bacterial population's survival in response to stressful environments.

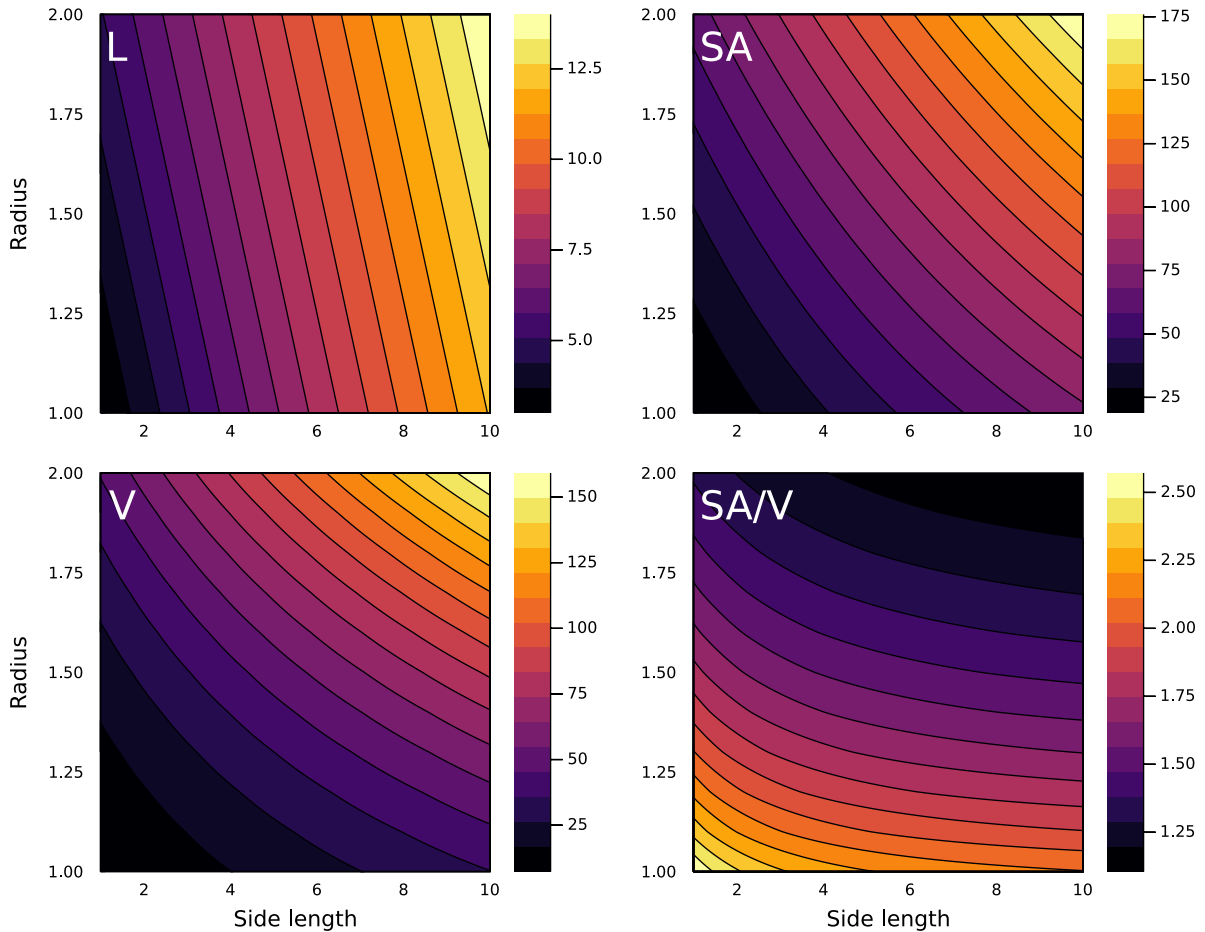


Figure 3.1: **Cell dimensions relationship.** We evaluated the resulting geometric properties on a grid of side lengths and radii with a pill-shaped cell. We can see that by maintaining a constant radius (typical case in bacteria such as *E. coli*) and increasing the side length, the surface area / volume relationship (SA/V) tends to decline since the V will grow at a higher rate than the SA .

3.2 Filamentation model

Let us assume the shape of cells is a cylinder with hemispherical ends. Based on this geometric structure, a nonlinear system of differential equations governing filamentation can be written as follows:

$$\begin{aligned}\frac{dT_{int}}{dt} &= T_{sa} \cdot (T_{ext}(t) - T_{vol}) - \alpha \cdot T_{ant} \cdot T_{int} \\ \frac{dL}{dt} &= \begin{cases} \beta \cdot L, & \text{if } T_{int} \geq T_{sos}, t \geq \tau_{sos} + \tau_{delay} \text{ and } L < L_{max} \\ 0, & \text{otherwise} \end{cases}\end{aligned}\quad (3.1)$$

It considers the internal toxin (T_{int}) and the cell length (L) as variables. T_{sa} and T_{vol} represent the surface area and volume of the toxin in the cell, respectively. $T_{ext}(t)$ is a function that returns the amount of toxin in the cell medium. T_{anti} and α symbolize the amount of antitoxin and its efficiency rate, respectively. β as the rate of filamentation. L_{max} is the maximum size that the cell can reach when filamentation is on. T_{sos} and T_{kill} are thresholds for filamentation and death, respectively. Finally, τ_{delay} is the amount of time required to activate filamentation after reaching the T_{sos} threshold.

3.3 Numerical results

3.3.1 Filamentation provides transient resistance to stressful conditions

When growing rod-shaped bacterial cells under constant conditions, the distribution of lengths and radii is narrow (Schaechter et al. 1962). However, when growing under stress conditions, some cells produce filaments (Schaechter, MaalOe, and Kjeldgaard 1958). This phenomenon may depend on the SOS response system (Bos et al. 2015), which can repair DNA damage, giving the cell greater chances of recovering and surviving under stress conditions. Besides, the SOS response has been reported to have precise temporal coordination in individual bacteria (Friedman et al. 2005). Among the stress conditions that can trigger the SOS response is exposure to beta-lactam antibiotics (Miller 2004).

In general, filamentation has been studied as an unavoidable consequence of stress. However, we considered filamentation an active process that produces the first line of defense against toxic agents. Therefore, a differential equation model was proposed that assesses the change in the amount of internal toxin as a function of cell length. At the core of this model, we include the intrinsic relationship between the surface area and the capsule volume since it is vital in determining cell size (L. K. Harris and Theriot 2016).

In Figure 3.2, cells grow in a ramp-shaped external toxin signal without considering a toxin-antitoxin system. As time progresses, the toxin in the external environment increases, so the cell raises its internal toxin levels. At approximately time 22, any cell reaches T_{sos} . The control cell (unable to filament) and the average cell (capable of filamenting) reach

the death threshold, T_{kill} , at times 31 and 93 (hatched and solid black lines), respectively. Therefore, under this example, the cell has increased its life span three times more than in control by growing as a filament (green shaded area versus orange shaded area). In turn, Figure 3.2 also shows stochastic simulations of the system in the intake of internal toxins. Considering that cell growth and death processes are inherently stochastic, stochastic simulations would be a better approximation. However, from now on, we will continue with the study of the deterministic model.

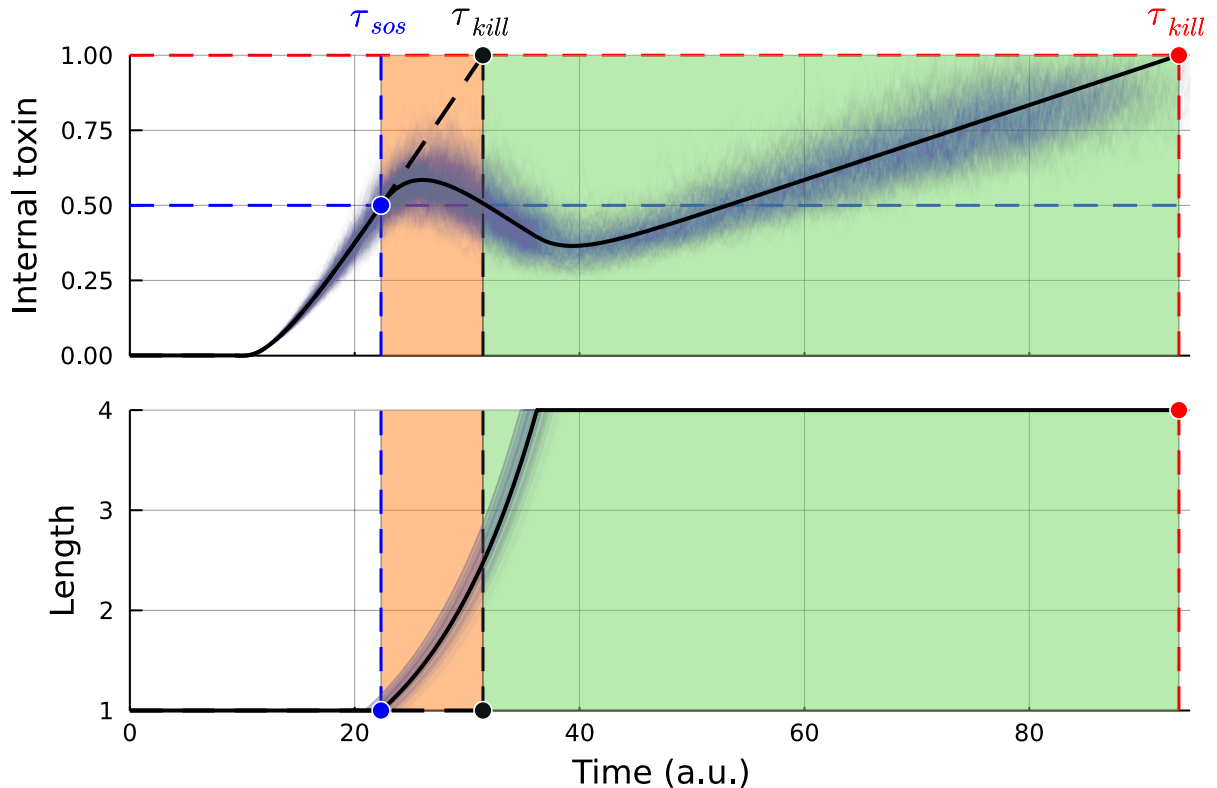


Figure 3.2: Effect of filamentation on intracellular toxin concentration. In the presence of an extracellular toxic agent, the intracellular concentration of the toxin (T_{int}) increases until reaching a damage threshold that triggers filamentation (T_{sos} , blue point), increasing cell length (L). When filamentation is on, the cell decreases T_{int} due to the intrinsic relationship between surface area and cell volume. When the cell reaches its maximum length, it eventually dies if the stressful stimulus is not removed (T_{kill} , red dot). The hatched line represents a cell that can not grow as filament. The orange shaded area is the time between stress and the non-filament cell's death, while the green shaded area represents the temporal gain for doing so. The blue background lines represent stochastic simulations of the same system.

3.3.2 Filamentation increases the minimum inhibitory concentration

In order to characterize the degree of resistance, dose-response experiments determine the Minimum Inhibitory Concentration (MIC) ([Jennifer M. Andrews 2001](#); [J. M. Andrews 2002](#)). Bacteria are capable of modifying their MIC through various mechanisms, for example, mutations ([Lambert 2005](#)), impaired membrane permeability ([Sato and Nakae 1991](#)), flux pumps ([Webber 2003](#)), toxin-inactivating enzymes ([Wright 2005](#)), and plasticity phenotypic ([Sheryl S. Justice et al. 2008](#)). The latter is our phenomenon of interest because it considers the change in shape and size, allowing us to study it as a strategy to promote bacterial survival.

We decided to analyze the MIC change caused by filamentation through stable exposure experiments of different toxin amounts at other exposure times. Computational simulations show that when comparing cells unable to filament with those that can, there is an increase in the capacity to tolerate more generous amounts of toxin, increasing their MIC (see Figure 3.3). Therefore, it confers a gradual increase in resistance beyond filamentation's role in improving the cell's life span as the exposure time is longer.

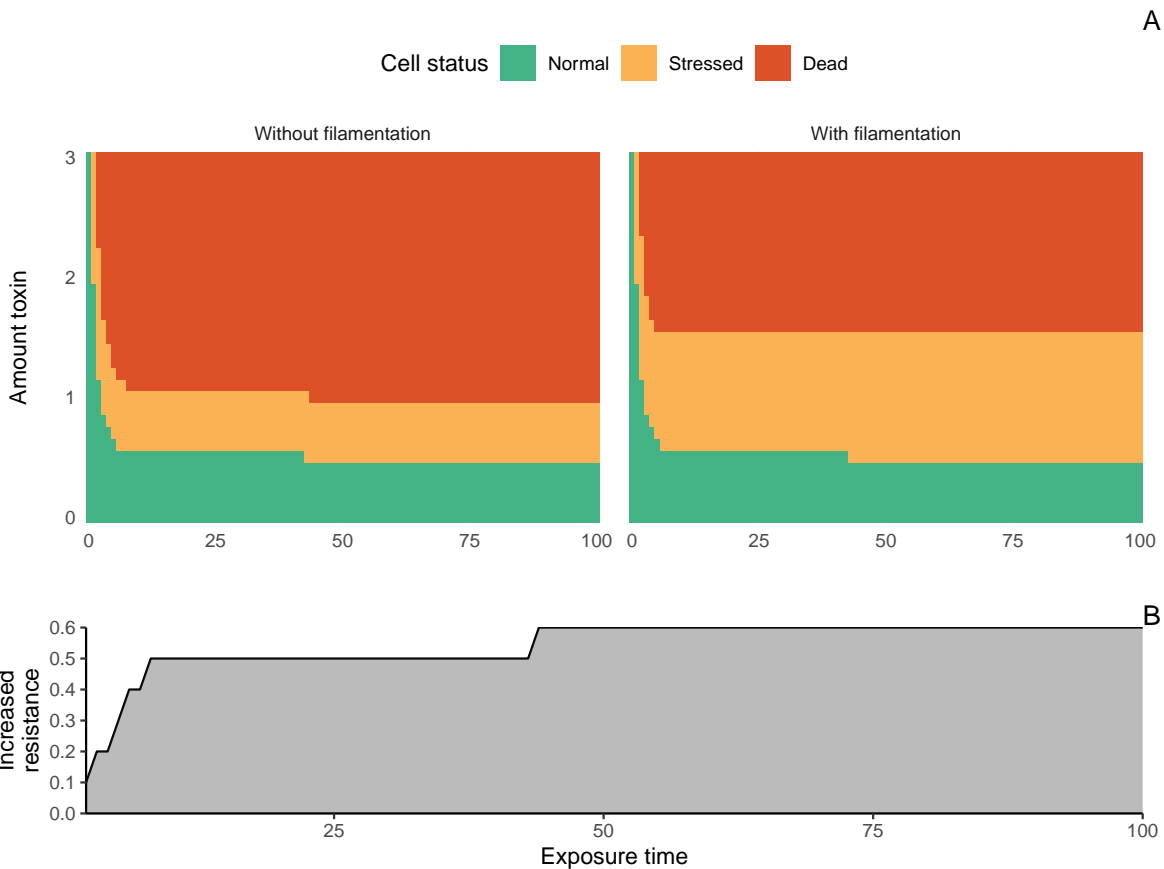


Figure 3.3: **Effect of filamentation on minimum inhibitory concentration (MIC).**

By exposing a cell to different toxin concentrations with stable signals, the cell achieves a set MIC for conditions without or with filamentation (separation between stressed and dead state) for each exposure time, without representing a change for the normal state cells' points (blue zone). Thus, the green line represents a gradual MIC increase when comparing each MIC between conditions for each exposure time.

3.3.3 Heterogeneity in the toxin-antitoxin system represents a double-edged sword in survival probability

One of the SOS response system properties is that it presents synchronous activation times within homogeneous populations (Friedman et al. 2005). It has constant gene expression rates that help it cope with stress; however, it is possible to introduce variability by considering having multicopy resistance plasmids (Million-Weaver and Camps 2014).

Therefore, the response times would have an asynchronous behavior at the global level but synchronous at the local level.

To include this observation into the model, we include a negative term to the internal toxin representing a toxin-antitoxin system. Therefore, the model now has an efficiency rate of the antitoxin and a stable amount per cell. We simulate the effect of the toxin-antitoxin system variation within a 1000-cell population; we initialize each one with similar initial conditions, except for the amount of internal antitoxin, defined as $T_{anti} \sim N(\mu, \sigma)$. Considering that T_{anti} values < 0 are equal to 0. For each experiment, $\mu = 25$, while it was evaluated in the range $[0 - 20]$. For the generation of pseudo-random numbers and to ensure the results' reproducibility, the number 42 was considered seed.

As shown in Figure Figure 3.4), when we compare heterogeneous populations in their toxin-antitoxin system, we can achieve different population dynamics, that is, changes in the final proportions of cell states; normal, stressed, and dead. This difference is because the cell sometimes has more or less antitoxin to handle the incoming stress situation.

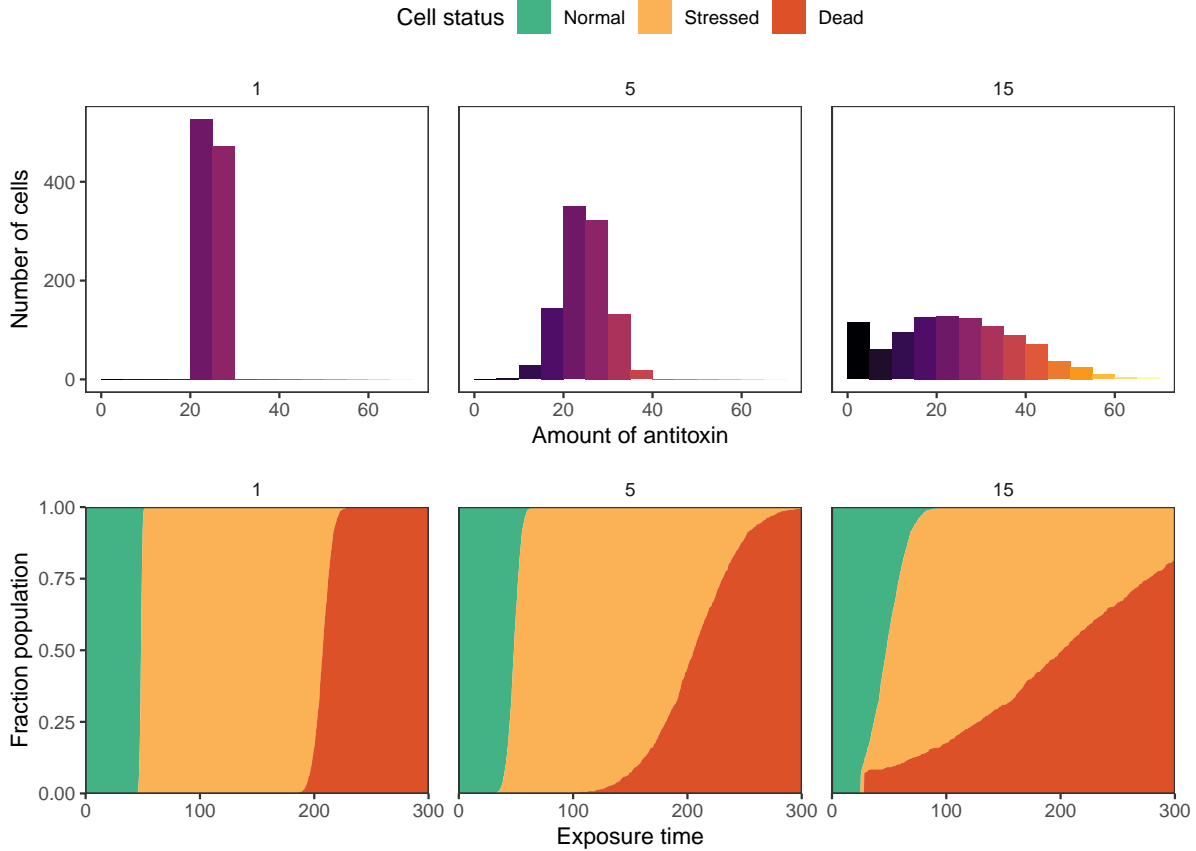


Figure 3.4: Variability in the toxin-antitoxin system produces different proportions of cell states. Histograms represent the distribution of antitoxin quantity, while the curves represent the population's fraction over time. The cell will start to filament after reaching a certain internal toxin threshold, T_{sos} . Therefore, the expected global effect on the population's response times based on the amount of antitoxin is asynchronous, while at the local level, it is synchronous. Consequently, different proportions are presented in the cellular states since some cells will activate the filamentation system before and others later.

Considering that the toxin-antitoxin system's variability can modify the proportions of final cell states, a question arose about heterogeneity levels' global behavior. To answer this question, we evaluate the probability of survival for each population, defined by its distribution of antitoxin levels. In this way, we characterized the population survival probability function into three essential points according to its effect: negative, invariant, and positive (see Figure 3.5). Furthermore, these points are relative to the homogeneous

population's death time in question (τ_{kill}): when $t < \tau_{kill}$ will represent a detrimental effect on survival, $t = \tau_{kill}$ will be independent of variability, and $t > \tau_{kill}$ will be a beneficial point for survival. Therefore, we concluded that the effect of heterogeneity in a toxin-antitoxin system represents a double-edged sword.

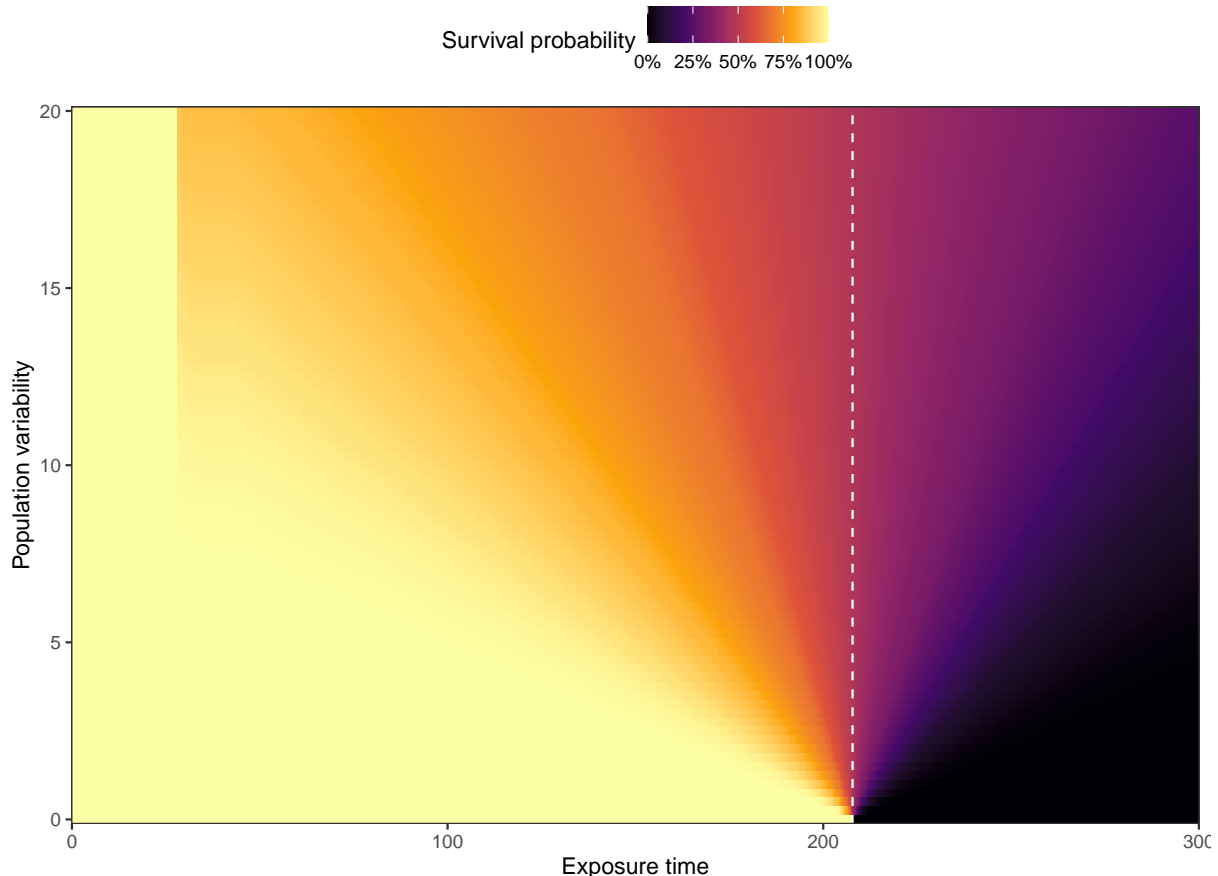


Figure 3.5: Effect of variability on the toxin-antitoxin system. The color of the heatmap is representative of the fraction of living cells at exposure time. The white vertical line represents the death time of the homogeneous population (τ_{kill}). At $t < \tau_{kill}$, it is shown that the fraction of survivors decreases as the variability in the population increases. When $t = \tau_{kill}$, the variability does not affect the fraction of survivors, but it represents a percentage improvement for the homogeneous population. Finally, when $t > \tau_{kill}$, the heterogeneity of the population favors survival.

3.4 Benefits and limitations of the model

Today, there have been advancements in the number of techniques that have allowed it to extend quantitative analyses to individual cells' dynamic observations ([Campos et al. 2014](#); [Meldrum 2005](#); [Sliusarenko et al. 2011](#); [Taheri-Araghi et al. 2017](#); [Ursell et al. 2017](#)). Therefore, studying their cellular behavior every day from medium to medium can be somewhat reproducible, facilitating the association of complex biological functions in simple mathematical equations ([Neidhardt 1999](#)).

Here, we proposed a mathematical model showing that filamentation could serve as a population's resilience mechanism to stress conditions. Finding that filamentation's net effect generates an additional window of time for the cell to survive, decreasing the toxin's intracellular concentration. However, we also found that a side effect of filamentation is to increase the cell's minimum inhibitory concentration. On the other hand, when we introduce variability in the amount of antitoxin in a cell population, we found that heterogeneity can be a double-edged sword, sometimes detrimental and sometimes beneficial, depending on the time of exposure to the toxic agent.

Due to the above, despite being simple, the model could have the ability to recapitulate the behavior seen in nature from variables that we can calculate easily with single-cell measurements. However, in other situations, it could be helpful to consider the addition of variables such as cell wall production and peptidoglycans' accumulation, among others. Notwithstanding the lack of parameters that are a little closer to reality, confirming that the model can work under experimental conditions would represent an achievement due to its explanatory simplicity, starting, in this way, the path of the study of filamentation oriented to the ecology of stress.

4 Discussion

Bacterial cell survival is part of a complex biological system, which is one of the fundamental problems of the health sector in this century. In this work, we have analyzed the role of filamentation in cell survival through multiple levels of complexity. Inquiring, one step at a time, into the ecology of bacterial stress.

First, we exposed two bacterial strains, one with an antibiotic resistance gene on the chromosome and one on multicopy plasmids, in a stressful environment with ampicillin. In both cases, we observed four states in the cells at the end of the experiment: live filamented, live non-filamented, dead filamented, and dead non-filamented cells. By inspecting the specific characteristics of each category, we were able to identify that cell length was indeed related to the probability of survival. In addition, we showed that each cell's inherent resistance defined whether or not filamentation would occur for the plasmid strain, where low resistance values were conducive to filamentation.

However, the growth rate was critical in determining the final cellular state. We observed that moderate growths mainly were related to survival. In contrast, rapid growth was associated with cell death. Previous findings, in addition, could have other explanations that are not mutually exclusive, such as the cell cycle or how fast a given cell was dividing. So the contribution of these variables in conjunction with filamentation could be a future study of interest to improve our understanding of cell survival.

Our next step was to abstract the fundamental information to define a mathematical model that would help us better understand the workings of filamentation in cell survival. We postulated a mathematical model built from a system of differential equations that considers the cell's geometric relationships (i.e., a pill shape) against exposure to a toxic substance in the environment. We assume that the consumption of antibiotics by the cell is perceived through its surface area (SA), while the cell volume (V) defines its concentration. Consequently, since the rate of change of SA is lower than V , this results in a transient reduction in the intracellular concentration of the toxin.

In the experiments, we showed how cells begin to filament upon a pulse of antibiotics, and from this, it would begin their bid for survival. The model allowed us to consider thousands of different cells to precisely determine the impact of filamentation on their survival. For instance, upon incremental exposure to the toxic substance, a cell can

increase its lifetime window by simply growing. If the antibiotic wears off before the cell reaches a threshold of death for some reason, it will have paid off; the cell will have won the bet, and it will have survived. Conversely, if a cell can not grow as a filament, it will depend entirely on its inherent resistance levels.

In addition to the increase in the expected lifetime of the cell upon exposure to a toxic agent, the model showed us that filamentation could confer an increase in the Minimum Inhibitory Concentration (MIC). So if a cell can grow as filament, a higher amount of the toxic agent will be needed to kill it. However, bacteria generally live in heterogeneous populations, and sometimes their inherent resistance levels will play a vital role in their survival.

The model showed us that heterogeneity in toxin-antitoxin response systems could represent a double-edged sword for cell survival depending on the time of exposure to the toxin. Heterogeneity could be favorable for survival if the time of exposure to the toxic agent is longer than the time at which the population without heterogeneity dies completely, while it would be detrimental otherwise. Thus, globally, filamentation, both at the individual and population scale, is crucial for resilience.

However, although our model's advantages are its simplicity, ease of interpretation, and reproducibility of the biological phenomenon in question, it also entails limitations to be considered in further work.

Our model assumes zero growth if the cell does not reach the filamentation threshold. While this may be true at the population average level, the reality is that cells are constantly growing and dividing. Integrating constant growth and division events could help us understand in more detail how, under what conditions, and why filamentation might be beneficial or detrimental when considering new transition states.

Another limiting factor is the lack of a system that penalizes prolonged filamentation. Once the cell filaments, our model considers only two possible scenarios, the cell can either continue with filamentation for its entire lifetime or die from crossing a toxic agent threshold. However, we can suggest that maintaining a filamentary state carries an energetic and membrane material cost that may be difficult to supply. Thus, a cell could die from spending too long in the filamentation state if exposure to the toxic agent does not cease.

The model does not consider what happens after the death of a cell or its interactions with other population members. We could hypothesize different scenarios: for instance, filament cells could absorb a more significant amount of the toxic agent so that some surrounding cells will not perceive much threat. On the other hand, if a cell dies, eventually, the capabilities of the cell membrane disappear, and its contents can diffuse into the environment. Hence, this would represent an increase in the toxic agent's local concentration that nearby cells could acquire. How would this change the overall dynamics

of the system? What would be the new cellular states when evaluating filamentation in the context of cellular communities?

In conclusion, although we based our model on experimental evidence, it does not consider all possible biological aspects. However, this allowed us to analyze and better understand filamentation as a mechanism capable of increasing the resilience of a bacterial population against a toxic agent exposure, for example, antibiotics. Therefore, the generation of new models and experiments to understand filamentation in-depth and its implications for bacterial survival will be necessary to help us combat the current problem of antibiotic resistance.

Appendix

Code availability

All code that we used in each phase of the project can be located on Github. Below we listed the repositories used as well as a brief description of their content.

Table 4.1: Github repositories used for this project.

Repository	Description
https://github.com/ccg-esb-lab/uJ	It contains a series of programs in μ J, which consist of an <i>ImageJ</i> macro library for quantifying unicellular bacterial dynamics in microfluidic devices. Besides, it includes all the Python code used for the image analysis processing and our developed custom Napari cell-viewer (see Chapter 1).
https://github.com/jvelezmagic/undergraduate_research_project	It contains all the files necessary to reproduce this document in its entirety. In addition, it includes the code used in R to analyze the tabular data of the experiments (see Chapter 2).
https://github.com/jvelezmagic/CellFilamentation	In includes all the Julia code used to create the mathematical filamentation model exposed in Chapter 3.

Software tools

Python

Below is the main list of packages used for Chapter 1

- Python ([Van Rossum and Drake 2009](#)).

- dask ([Rocklin 2015](#)).
- ipython ([Pérez and Granger 2007](#)).
- matplotlib ([Hunter 2007](#)).
- napari ([Sofroniew et al. 2021](#)).
- networkx ([Hagberg, Swart, and S Chult 2008](#)).
- numpy ([C. R. Harris et al. 2020](#)).
- pandas ([McKinney et al. 2010](#)).
- pickle ([Van Rossum 2020](#)).
- scikit-image ([van der Walt et al. 2014](#)).
- shapely ([Gillies et al. 2007--](#)).

R

Below is the main list of packages used for Chapter 2 as well for the reproducibility of this undergraduate research project.

- base ([R Core Team 2022](#)).
- embed ([Hvitfeldt and Kuhn 2022](#)).
- fs ([Hester, Wickham, and Csárdi 2021](#)).
- GGally ([Schloerke et al. 2021](#)).
- ggdist ([Kay 2022](#)).
- ggpubr ([Kassambara 2020](#)).
- here ([Müller 2020](#)).
- janitor ([Firke 2021](#)).
- knitr ([Xie 2022](#)).
- patchwork ([Pedersen 2020](#)).
- plotly ([Sievert et al. 2021](#)).
- quarto ([Allaire 2022](#)).
- renv ([Ushey 2022](#)).
- rmarkdown ([Allaire et al. 2022](#)).
- sessioninfo ([Wickham et al. 2021](#)).
- stringr ([Wickham 2019](#)).
- tidymodels ([Kuhn and Wickham 2022](#)).
- tidytext ([Robinson and Silge 2022](#)).
- tidyverse ([Wickham 2022](#)).

Julia

Below is the main list of packages used for Chapter 3.

- Julia ([Bezanson et al. 2017](#)).
- DrWatson.jl ([Datseris et al. 2020](#)).
- DifferentialEquations.jl ([Rackauckas and Nie 2017b, 2017a, 2018](#)).
- DataFrames.jl ([White et al. 2021](#)).

Software usage

Undergraduate research project

This code base is using the R Language , Quarto, and `renv` to make a reproducible scientific project named `bacterial-filamentation-research`.

1. Clone the repository with: `git clone https://github.com/jvelezmagic/bacterial-filamentation-research`.
2. Download latest version of [R](#).
3. Download latest version of [Quarto](#).
4. Open R project.
5. Install the `renv` package with `install.packages('renv')`.
6. Restore working environment with: `renv::restore()`.
7. Render the book with: `quarto::quarto_render()`.
8. Edit documents and render again.

Cell-viewer

This code base is using the Python Language.

1. Clone the repository with: `git clone https://github.com/ccg-esb-lab/uJ`.
2. Go to `single-channel` directory.
3. Inside of `MGGT-AMP-Pulse` (*i.e.*, chromosome strain) or `pBGT-AMP-Pulse` (*i.e.*, plasmid strain) enter to `6_Lineages_corrector_napari.ipynb`.
4. Change the parameters and use it.

Filamentation model

This code base is using the Julia Language and DrWatson to make a reproducible scientific project named `CellFilamentation`.

1. Clone the repository with: `git clone https://github.com/jvelezmagic/CellFilamentation`.
2. Download latest version of [Julia](#).

3. Open Julia project.
4. Open Julia console and do the following to restore working environment:

```
using Pkg
Pkg.activate(".") # Path to the project.
Pkg.instantiate()
```

5. Play with the model.

Colophon

This undergraduate research project was written in [RStudio](#) using [Quarto](#). The [website](#) is hosted via Github Pages, and the complete source is available via Github.

This version of the project was built with R version 4.2.0 (2022-04-22) and the following packages:

Table 4.2: Packages used to built the project documents.

Package	Version	Source
embed	1.0.0	CRAN (R 4.2.0)
fs	1.5.2	CRAN (R 4.2.0)
GGally	2.1.2	CRAN (R 4.2.0)
gddist	3.2.0	CRAN (R 4.2.0)
ggpubr	0.4.0	CRAN (R 4.2.0)
here	1.0.1	CRAN (R 4.2.0)
janitor	2.1.0	CRAN (R 4.2.0)
knitr	1.39	CRAN (R 4.2.0)
patchwork	1.1.1	CRAN (R 4.2.0)
plotly	4.10.0	CRAN (R 4.2.0)
quarto	1.2	CRAN (R 4.2.0)
renv	0.15.5	CRAN (R 4.2.0)
rmarkdown	2.14	CRAN (R 4.2.0)
sessioninfo	1.2.2	CRAN (R 4.2.0)
stringr	1.4.0	CRAN (R 4.2.0)
tidymodels	1.0.0	CRAN (R 4.2.0)
tidytext	0.3.3	CRAN (R 4.2.0)
tidyverse	1.3.2	CRAN (R 4.2.0)

References

- Ackermann, Martin. 2015. “A Functional Perspective on Phenotypic Heterogeneity in Microorganisms.” *Nature Reviews Microbiology* 13 (8): 497–508. <https://doi.org/10.1038/nrmicro3491>.
- Allaire, JJ. 2022. *Quarto: R Interface to Quarto Markdown Publishing System*. <https://github.com/quarto-dev/quarto-r>.
- Allaire, JJ, Yihui Xie, Jonathan McPherson, Javier Luraschi, Kevin Ushey, Aron Atkins, Hadley Wickham, Joe Cheng, Winston Chang, and Richard Iannone. 2022. *Rmarkdown: Dynamic Documents for r*. <https://CRAN.R-project.org/package=rmarkdown>.
- Altman, N. S. 1992. “An Introduction to Kernel and Nearest-Neighbor Nonparametric Regression.” *The American Statistician* 46 (3): 175–85. <https://doi.org/10.1080/00031305.1992.10475879>.
- Andersson, Dan I. 2005. “The Ways in Which Bacteria Resist Antibiotics.” *International Journal of Risk and Safety in Medicine* 17 (3-4): 111–16.
- Andrews, J. M. 2002. “Determination of Minimum Inhibitory Concentrations.” *Journal of Antimicrobial Chemotherapy* 49 (6): 1049–49. <https://doi.org/10.1093/jac/dkf083>.
- Andrews, Jennifer M. 2001. “Determination of Minimum Inhibitory Concentrations.” *Journal of Antimicrobial Chemotherapy* 48 (suppl_1): 5–16. https://doi.org/10.1093/jac/48.suppl_1.5.
- Balaban, Nathalie Q., Jack Merrin, Remy Chait, Lukasz Kowalik, and Stanislas Leibler. 2004. “Bacterial Persistence as a Phenotypic Switch.” *Science* 305 (5690): 1622–25. <https://doi.org/10.1126/science.1099390>.
- Bezanson, Jeff, Alan Edelman, Stefan Karpinski, and Viral B Shah. 2017. “Julia: A Fresh Approach to Numerical Computing.” *SIAM Review* 59 (1): 65–98. <https://doi.org/10.1137/141000671>.
- Bos, Julia, Qiucen Zhang, Saurabh Vyawahare, Elizabeth Rogers, Susan M. Rosenberg, and Robert H. Austin. 2015. “Emergence of Antibiotic Resistance from Multinucleated Bacterial Filaments.” *Proceedings of the National Academy of Sciences* 112 (1): 178–83. <https://doi.org/10.1073/pnas.1420702111>.
- Brinkmann, Ron. 2008. *The Art and Science of Digital Compositing, Second Edition: Techniques for Visual Effects, Animation and Motion Graphics (the Morgan Kaufmann Series in ... Morgan Kaufmann Series in Computer Graphics)*. 2nd ed. San Francisco, CA, USA: Morgan Kaufmann Publishers Inc.

- Bruggeman, Frank J., Jorrit J. Hornberg, Fred C. Boogerd, and Hans V. Westerhoff. 2007. "Introduction to Systems Biology." In, 1–19. Birkhäuser Basel. https://doi.org/10.1007/978-3-7643-7439-6_1.
- Caicedo, Juan C, Sam Cooper, Florian Heigwer, Scott Warchal, Peng Qiu, Csaba Molnar, Aliaksei S Vasilevich, et al. 2017. "Data-Analysis Strategies for Image-Based Cell Profiling." *Nature Methods* 14 (9): 849–63. <https://doi.org/10.1038/nmeth.4397>.
- Campos, Manuel, Ivan V. Surovtsev, Setsu Kato, Ahmad Paintdakhi, Bruno Beltran, Sarah E. Ebmeier, and Christine Jacobs-Wagner. 2014. "A Constant Size Extension Drives Bacterial Cell Size Homeostasis." *Cell* 159 (6): 1433–46. <https://doi.org/10.1016/j.cell.2014.11.022>.
- Cayron, Julien, Annick Dedieu, and Christian Lesterlin. 2020. "Bacterial Filament Division Dynamics Allows Rapid Post-Stress Cell Proliferation." <http://dx.doi.org/10.1101/2020.03.16.993345>.
- Convery, Neil, and Nikolaj Gadegaard. 2019. "30 Years of Microfluidics." *Micro and Nano Engineering* 2 (March): 76–91. <https://doi.org/10.1016/j.mne.2019.01.003>.
- Datseris, George, Jonas Isensee, Sebastian Pech, and Tamás Gál. 2020. "DrWatson: The Perfect Sidekick for Your Scientific Inquiries." *Journal of Open Source Software* 5 (54): 2673. <https://doi.org/10.21105/joss.02673>.
- Dever, L. A., and T. S. Dermody. 1991. "Mechanisms of bacterial resistance to antibiotics." *Archives of Internal Medicine* 151 (5): 886–95.
- "Editorial Board." 2014. *Journal of Global Antimicrobial Resistance* 2 (2): ii. [https://doi.org/10.1016/S2213-7165\(14\)00044-7](https://doi.org/10.1016/S2213-7165(14)00044-7).
- Elowitz, Michael B., Arnold J. Levine, Eric D. Siggia, and Peter S. Swain. 2002. "Stochastic Gene Expression in a Single Cell." *Science* 297 (5584): 1183–86. <https://doi.org/10.1126/science.1070919>.
- Firke, Sam. 2021. *Janitor: Simple Tools for Examining and Cleaning Dirty Data*. <https://github.com/sfirke/janitor>.
- Friedman, Nir, Shuki Vardi, Michal Ronen, Uri Alon, and Joel Stavans. 2005. "Precise Temporal Modulation in the Response of the SOS DNA Repair Network in Individual Bacteria." Edited by B'en'edicte Michel. *PLoS Biology* 3 (7): e238. <https://doi.org/10.1371/journal.pbio.0030238>.
- Gillies, Sean et al. 2007--. "Shapely: Manipulation and Analysis of Geometric Objects." [toblerity.org](https://github.com/Toblerity/Shapely). <https://github.com/Toblerity/Shapely>.
- Hagberg, Aric, Pieter Swart, and Daniel S Chult. 2008. "Exploring Network Structure, Dynamics, and Function Using NetworkX." Los Alamos National Lab.(LANL), Los Alamos, NM (United States).
- Harris, Charles R., K. Jarrod Millman, Stéfan J van der Walt, Ralf Gommers, Pauli Virtanen, David Cournapeau, Eric Wieser, et al. 2020. "Array Programming with NumPy." *Nature* 585: 357–62. <https://doi.org/10.1038/s41586-020-2649-2>.
- Harris, Leigh K., and Julie A. Theriot. 2016. "Relative Rates of Surface and Volume Synthesis Set Bacterial Cell Size." *Cell* 165 (6): 1479–92. <https://doi.org/10.1016/j>.

[cell.2016.05.045](#).

- Heinrich, Kristina, David J. Leslie, and Kristina Jonas. 2015. “Modulation of Bacterial Proliferation as a Survival Strategy.” In, 127–71. Elsevier. <https://doi.org/10.1016/bs.aambs.2015.02.004>.
- Hester, Jim, Hadley Wickham, and Gábor Csárdi. 2021. *Fs: Cross-Platform File System Operations Based on Libuv*. <https://CRAN.R-project.org/package=fs>.
- Hotelling, Harold. 1936. “Relations Between Two Sets of Variates.” *Biometrika* 28 (3/4): 321. <https://doi.org/10.2307/2333955>.
- Hunter, John D. 2007. “Matplotlib: A 2D Graphics Environment.” *Computing in Science & Engineering* 9 (3): 90–95.
- Hvitfeldt, Emil, and Max Kuhn. 2022. *Embed: Extra Recipes for Encoding Predictors*. <https://CRAN.R-project.org/package=embed>.
- Jaimes-Lizcano, Yuly A., Dayton D. Hunn, and Kyriakos D. Papadopoulos. 2014. “Filamentous Escherichia Coli Cells Swimming in Tapered Microcapillaries.” *Research in Microbiology* 165 (3): 166–74. <https://doi.org/10.1016/j.resmic.2014.01.007>.
- Joseleau-Petit, Danièle, Daniel Vinella, and Richard D’Ari. 1999. “Metabolic Alarms and Cell Division in Escherichia Coli.” *Journal of Bacteriology* 181 (1): 9–14. <https://doi.org/10.1128/jb.181.1.9-14.1999>.
- Justice, S. S., D. A. Hunstad, P. C. Seed, and S. J. Hultgren. 2006. “Filamentation by Escherichia Coli Subverts Innate Defenses During Urinary Tract Infection.” *Proceedings of the National Academy of Sciences* 103 (52): 19884–89. <https://doi.org/10.1073/pnas.0606329104>.
- Justice, Sheryl S., David A. Hunstad, Lynette Cegelski, and Scott J. Hultgren. 2008. “Morphological Plasticity as a Bacterial Survival Strategy.” *Nature Reviews Microbiology* 6 (2): 162–68. <https://doi.org/10.1038/nrmicro1820>.
- Kassambara, Alboukadel. 2020. *Ggpubr: Ggplot2 Based Publication Ready Plots*. <https://rpkg.datanovia.com/ggpubr/>.
- Kay, Matthew. 2022. *Ggdist: Visualizations of Distributions and Uncertainty*. <https://CRAN.R-project.org/package=ggdist>.
- Kroemer, G, L Galluzzi, P Vandebaele, J Abrams, E S Alnemri, E H Baehrecke, M V Blagosklonny, et al. 2008. “Classification of Cell Death: Recommendations of the Nomenclature Committee on Cell Death 2009.” *Cell Death & Differentiation* 16 (1): 3–11. <https://doi.org/10.1038/cdd.2008.150>.
- Kuhn, Max, and Hadley Wickham. 2022. *Tidymodels: Easily Install and Load the Tidymodels Packages*. <https://CRAN.R-project.org/package=tidymodels>.
- Lambert, P. 2005. “Bacterial Resistance to Antibiotics: Modified Target Sites.” *Advanced Drug Delivery Reviews* 57 (10): 1471–85. <https://doi.org/10.1016/j.addr.2005.04.003>.
- McInnes, Leland, John Healy, and James Melville. 2018. “Umap: Uniform Manifold Approximation and Projection for Dimension Reduction.” *arXiv Preprint arXiv:1802.03426*.

- McKinney, Wes et al. 2010. “Data Structures for Statistical Computing in Python.” In *Proceedings of the 9th Python in Science Conference*, 445:51–56. Austin, TX.
- Meldrum, Deirdre. 2005. “Faculty Opinions Recommendation of Bacterial Persistence as a Phenotypic Switch.” <https://doi.org/10.3410/f.1021664.264823>.
- Miller, C. 2004. “SOS Response Induction by -Lactams and Bacterial Defense Against Antibiotic Lethality.” *Science* 305 (5690): 1629–31. <https://doi.org/10.1126/science.1101630>.
- Million-Weaver, Samuel, and Manel Camps. 2014. “Mechanisms of Plasmid Segregation: Have Multicopy Plasmids Been Overlooked?” *Plasmid* 75 (September): 27–36. <https://doi.org/10.1016/j.plasmid.2014.07.002>.
- Moger-Reischer, Roy Z., and Jay T. Lennon. 2019. “Microbial Ageing and Longevity.” *Nature Reviews Microbiology* 17 (11): 679–90. <https://doi.org/10.1038/s41579-019-0253-y>.
- Mückl, Andrea, Matthaeus Schwarz-Schilling, Katrin Fischer, and Friedrich C. Simmel. 2018. “Filamentation and Restoration of Normal Growth in Escherichia Coli Using a Combined CRISPRi sgRNA/Antisense RNA Approach.” Edited by Mark Isalan. *PLOS ONE* 13 (9): e0198058. <https://doi.org/10.1371/journal.pone.0198058>.
- Müller, Kirill. 2020. *Here: A Simpler Way to Find Your Files*. <https://CRAN.R-project.org/package=here>.
- Neidhardt, Frederick C. 1999. “Bacterial Growth: Constant Obsession with dN/Dt .” *Journal of Bacteriology* 181 (24): 7405–8. <https://doi.org/10.1128/JB.181.24.7405-7408.1999>.
- Pearson, Karl. 1901. “LIII. On Lines and Planes of Closest Fit to Systems of Points in Space.” *The London, Edinburgh, and Dublin Philosophical Magazine and Journal of Science* 2 (11): 559–72. <https://doi.org/10.1080/14786440109462720>.
- Pedersen, Thomas Lin. 2020. *Patchwork: The Composer of Plots*. <https://CRAN.R-project.org/package=patchwork>.
- Pérez, Fernando, and Brian E Granger. 2007. “IPython: A System for Interactive Scientific Computing.” *Computing in Science & Engineering* 9 (3).
- R Core Team. 2022. *R: A Language and Environment for Statistical Computing*. Vienna, Austria: R Foundation for Statistical Computing. <https://www.R-project.org/>.
- Rackauckas, Christopher, and Qing Nie. 2017a. “Adaptive Methods for Stochastic Differential Equations via Natural Embeddings and Rejection Sampling with Memory.” *Discrete and Continuous Dynamical Systems. Series B* 22 (7): 2731.
- . 2017b. “Differentialequations.jl—a Performant and Feature-Rich Ecosystem for Solving Differential Equations in Julia.” *Journal of Open Research Software* 5 (1).
- . 2018. “Stability-Optimized High Order Methods and Stiffness Detection for Pathwise Stiff Stochastic Differential Equations.” *arXiv:1804.04344 [Math]*. <http://arxiv.org/abs/1804.04344>.
- Robinson, David, and Julia Silge. 2022. *Tidytext: Text Mining Using Dplyr, Ggplot2, and Other Tidy Tools*. <https://github.com/juliasilge/tidytext>.

- Rocklin, Matthew. 2015. “Dask: Parallel Computation with Blocked Algorithms and Task Scheduling.” In *Proceedings of the 14th Python in Science Conference*. 130–136. Citeseer.
- Roostalu, Johanna, Arvi Jõers, Hannes Luidalepp, Niilo Kaldalu, and Tanel Tenson. 2008. “Cell Division in Escherichia Colicultures Monitored at Single Cell Resolution.” *BMC Microbiology* 8 (1). <https://doi.org/10.1186/1471-2180-8-68>.
- San Millan, Alvaro, Jose Antonio Escudero, Danna R. Gifford, Didier Mazel, and R. Craig MacLean. 2016. “Multicopy Plasmids Potentiate the Evolution of Antibiotic Resistance in Bacteria.” *Nature Ecology & Evolution* 1 (1). <https://doi.org/10.1038/s41559-016-0010>.
- Sato, Kazuhito, and Taiji Nakae. 1991. “Outer Membrane Permeability of *Acinetobacter Calcoaceticus* and Its Implication in Antibiotic Resistance.” *Journal of Antimicrobial Chemotherapy* 28 (1): 35–45. <https://doi.org/10.1093/jac/28.1.35>.
- Schaechter, M., O. MaalOe, and N. O. Kjeldgaard. 1958. “Dependency on Medium and Temperature of Cell Size and Chemical Composition During Balanced Growth of *Salmonella Typhimurium*.” *Journal of General Microbiology* 19 (3): 592–606. <https://doi.org/10.1099/00221287-19-3-592>.
- Schaechter, M., J. P. Williamson, J. R. Hood, and A. L. Koch. 1962. “Growth, Cell and Nuclear Divisions in Some Bacteria.” *Journal of General Microbiology* 29 (3): 421–34. <https://doi.org/10.1099/00221287-29-3-421>.
- Schermelleh, Lothar, Alexia Ferrand, Thomas Huser, Christian Eggeling, Markus Sauer, Oliver Biehlmaier, and Gregor P. C. Drummen. 2019. “Super-Resolution Microscopy Demystified.” *Nature Cell Biology* 21 (1): 72–84. <https://doi.org/10.1038/s41556-018-0251-8>.
- Schloerke, Barret, Di Cook, Joseph Larmarange, Francois Briatte, Moritz Marbach, Edwin Thoen, Amos Elberg, and Jason Crowley. 2021. *GGally: Extension to Ggplot2*. <https://CRAN.R-project.org/package=GGally>.
- Schneider, Caroline A, Wayne S Rasband, and Kevin W Eliceiri. 2012. “NIH Image to ImageJ: 25 Years of Image Analysis.” *Nature Methods* 9 (7): 671–75. <https://doi.org/10.1038/nmeth.2089>.
- Sievert, Carson, Chris Parmer, Toby Hocking, Scott Chamberlain, Karthik Ram, Marianne Corvellec, and Pedro Despouy. 2021. *Plotly: Create Interactive Web Graphics via Plotly.js*. <https://CRAN.R-project.org/package=plotly>.
- Sliusarenko, Oleksii, Jennifer Heinritz, Thierry Emonet, and Christine Jacobs-Wagner. 2011. “High-Throughput, Subpixel Precision Analysis of Bacterial Morphogenesis and Intracellular Spatio-Temporal Dynamics: Quantitative Analysis of Spatio-Temporal Dynamics.” *Molecular Microbiology* 80 (3): 612–27. <https://doi.org/10.1111/j.1365-2958.2011.07579.x>.
- Smith, Kevin, Filippo Piccinini, Tamas Balassa, Krisztian Koos, Tivadar Danka, Hossein Azizpour, and Peter Horvath. 2018. “Phenotypic Image Analysis Software Tools for Exploring and Understanding Big Image Data from Cell-Based Assays.” *Cell Systems*

- 6 (6): 636–53. <https://doi.org/10.1016/j.cels.2018.06.001>.
- Sofroniew, Nicholas, Talley Lambert, Kira Evans, Juan Nunez-Iglesias, Grzegorz Bokota, Gonzalo Peña-Castellanos, Philip Winston, et al. 2021. *Napari/Napari: 0.4.12rc2*. Zenodo. <https://doi.org/10.5281/ZENODO.3555620>.
- Specht, Elizabeth A., Esther Braselmann, and Amy E. Palmer. 2017. “A Critical and Comparative Review of Fluorescent Tools for Live-Cell Imaging.” *Annual Review of Physiology* 79 (1): 93–117. <https://doi.org/10.1146/annurev-physiol-022516-034055>.
- Taheri-Araghi, Sattar, Serena Bradde, John T. Sauls, Norbert S. Hill, Petra Anne Levin, Johan Paulsson, Massimo Vergassola, and Suckjoon Jun. 2017. “Cell-Size Control and Homeostasis in Bacteria.” *Current Biology* 27 (9): 1392. <https://doi.org/10.1016/j.cub.2017.04.028>.
- Trevors, J.T. 2012. “Can Dead Bacterial Cells Be Defined and Are Genes Expressed After Cell Death?” *Journal of Microbiological Methods* 90 (1): 25–28. <https://doi.org/10.1016/j.mimet.2012.04.004>.
- TURING, A. M. 1950. “I.—COMPUTING MACHINERY AND INTELLIGENCE.” *Mind* LIX (236): 433–60. <https://doi.org/10.1093/mind/lix.236.433>.
- Ursell, Tristan, Timothy K. Lee, Daisuke Shiomi, Handuo Shi, Carolina Tropini, Russell D. Monds, Alexandre Colavin, et al. 2017. “Rapid, Precise Quantification of Bacterial Cellular Dimensions Across a Genomic-Scale Knockout Library.” *BMC Biology* 15 (1): 17. <https://doi.org/10.1186/s12915-017-0348-8>.
- Ushey, Kevin. 2022. *Renv: Project Environments*. <https://rstudio.github.io/renv/>.
- van der Walt, Stéfan, Johannes L. Schönberger, Juan Nunez-Iglesias, François Boulogne, Joshua D. Warner, Neil Yager, Emmanuelle Gouillart, and Tony Yu. 2014. “Scikit-Image: Image Processing in Python.” *PeerJ* 2 (June): e453. <https://doi.org/10.7717/peerj.453>.
- Van Rossum, Guido. 2020. *The Python Library Reference, Release 3.8.2*. Python Software Foundation.
- Van Rossum, Guido, and Fred L. Drake. 2009. *Python 3 Reference Manual*. Scotts Valley, CA: CreateSpace.
- Van Valen, David A., Takamasa Kudo, Keara M. Lane, Derek N. Macklin, Nicolas T. Quach, Mialy M. DeFelice, Inbal Maayan, Yu Tanouchi, Euan A. Ashley, and Markus W. Covert. 2016. “Deep Learning Automates the Quantitative Analysis of Individual Cells in Live-Cell Imaging Experiments.” Edited by Martin Meier-Schellersheim. *PLOS Computational Biology* 12 (11): e1005177. <https://doi.org/10.1371/journal.pcbi.1005177>.
- Verschaffel, Lieven, Brian Greer, and Erik de Corte. 2002. “Everyday Knowledge and Mathematical Modeling of School Word Problems.” In, 257–76. Springer Netherlands. https://doi.org/10.1007/978-94-017-3194-2_16.
- Wang, Jue D., and Petra A. Levin. 2009. “Metabolism, Cell Growth and the Bacterial Cell Cycle.” *Nature Reviews Microbiology* 7 (11): 822–27. <https://doi.org/10.1038>

nrmicro2202.

- Wang, Ying, Hong Wu, Xiaoran Jiang, and Guo-Qiang Chen. 2014. “Engineering Escherichia Coli for Enhanced Production of Poly(3-Hydroxybutyrate-Co-4-Hydroxybutyrate) in Larger Cellular Space.” *Metabolic Engineering* 25 (September): 183–93. <https://doi.org/10.1016/j.ymben.2014.07.010>.
- Wang, Ying, Jin Yin, and Guo-Qiang Chen. 2014. “Polyhydroxyalkanoates, Challenges and Opportunities.” *Current Opinion in Biotechnology* 30 (December): 59–65. <https://doi.org/10.1016/j.copbio.2014.06.001>.
- Webber, M. A. 2003. “The Importance of Efflux Pumps in Bacterial Antibiotic Resistance.” *Journal of Antimicrobial Chemotherapy* 51 (1): 9–11. <https://doi.org/10.1093/jac/dkg050>.
- White, John Myles, Bogumił Kamiński, Powerdistribution, Milan Bouchet-Valat, Sean Garborg, Jacob Quinn, Simon Kornblith, et al. 2021. *JuliaData/DataFrames.jl: V1.2.2*. Zenodo. <https://doi.org/10.5281/ZENODO.3376177>.
- Wickham, Hadley. 2019. *Stringr: Simple, Consistent Wrappers for Common String Operations*. <https://CRAN.R-project.org/package=stringr>.
- . 2022. *Tidyverse: Easily Install and Load the Tidyverse*. <https://CRAN.R-project.org/package=tidyverse>.
- Wickham, Hadley, Winston Chang, Robert Flight, Kirill Müller, and Jim Hester. 2021. *Sessioninfo: R Session Information*. <https://CRAN.R-project.org/package=sessioninfo>.
- Wright, G. 2005. “Bacterial Resistance to Antibiotics: Enzymatic Degradation and Modification.” *Advanced Drug Delivery Reviews* 57 (10): 1451–70. <https://doi.org/10.1016/j.addr.2005.04.002>.
- Xie, Yihui. 2022. *Knitr: A General-Purpose Package for Dynamic Report Generation in r*. <https://yihui.org/knitr/>.
- Yin, Huabing, and Damian Marshall. 2012. “Microfluidics for Single Cell Analysis.” *Current Opinion in Biotechnology* 23 (1): 110–19. <https://doi.org/10.1016/j.copbio.2011.11.002>.